UC Berkeley
SEMM Reports Series

Title

A generalized elasto-plastic plate theory and its algorithmic implementation

Permalink

https://escholarship.org/uc/item/1np3s9zt

Authors

Auricchio, Ferdinando

Taylor, Robert

Publication Date

1993-04-01

REPORT NO.
UCB/SEMM-93/04

A GENERALIZED ELASTO-PLASTIC PLATE THEORY AND ITS ALGORITHMIC IMPLEMENTATION

by

FERDINANDO AURICCHIO

and

ROBERT L. TAYLOR

APR 1993

DEPARTMENT OF CIVIL ENGINEERING
UNIVERSITY OF CALIFORNIA
BERKELEY, CALIFORNIA

A GENERALIZED ELASTO-PLASTIC PLATE THEORY AND ITS ALGORITHMIC IMPLEMENTATION

F.Auricchio   R.L.Taylor

Department of Civil Engineering

University of California at Berkeley, Berkeley, CA 94720 USA

Abstract

In continuum mechanics within specific classes of problems one or two dimensional theories are often simpler to apply then the more complete three dimensional one. This is for example the case of thin bodies, such as plates or shells, which may be studied using appropriate two dimensional theories.

Within this approach, the reduction of the dimension is traded for a loss of information relative to the motion in the transverse direction. For example in the case of non-linear material behavior, classical plasticity plate theories are usually not able to model the effects related to the spreading of plasticity through the cross section.

In the present paper we discuss a *generalized plasticity* plate model, which can be used to reproduce in a two dimensional setting some of the three dimensional effects. We present the continuous and the discrete time model, including both isotropic and kinematic hardening mechanisms; moreover, the form of the tangent matrix consistent with the discrete model is addressed.

Finally, some examples (cantilever beam, clamped circular plate and clamped square plate under monotonic and cyclic loading) are studied numerically using a three dimensional classical plasticity theory, a classical plasticity plate theory and the proposed plate theory. The generalized plasticity plate model matches the three dimensional response with greater accuracy, then the classical plasticity plate model.

1   INTRODUCTION

In continuum mechanics the most appropriate way to fully study the response of any body is clearly within a three dimensional theory. However, such analyses may often be a non trivial task to perform (consider for examples the effort needed to generate a finite element mesh and the computational cost for the solutions), especially if non linear material constitutive equations and/or complex loading patterns are considered. Accordingly, simpler theories can be of interest; as an example, for a shell or a plate, the particular geometry of the body may render appropriate the use of a two dimensional theory. In this case the loss of some information relative to the motion of the body in the transverse direction (such as cross section warping or thickness change) [1] is traded for a reduction of the dimension of the problem, hence of the ease and the speed at which analyses can be performed.

Similarly, under the assumption of inelastic material behavior, plate theories are often unable to simulate all the effects due the real three dimensionality of the problem, such as those connected to the diffusion of the plasticity through the cross section. In the present work, we introduce a new plasticity model, which is able to model some of the three dimensional inelastic effects, usually lost in a classical inelastic plate theory. We call the new model *generalized plasticity*, since it includes as a sub case the classical plasticity plate model.

The paper is organized as follow. We start by presenting the basic framework of our plasticity model, such as geometry, kinematics, kinetics and constitutive assumptions. In Section 3, we briefly consider the variational structure in which the elasto-plastic plate problem may be cast. In Section 4 we present the yield and the limit functions for the generalized plasticity model. Hence, the corresponding discrete model is described, as well as the finite element approximation and the related solution technique. To show the performance of the proposed plate model, we present some numerical examples; in particular, a cantilever beam, a clamped circular plate and a clamped square plate under monotonic and cyclic loading are analyzed using a three dimensional classical plasticity model, a classical plasticity plate model and

---

[1]The most common plate theories such as Reissner-Mindlin and Kirchhoff are unable to predict effects as the warping of the cross section or the change of the thickness. However, for the case of linear elastic solids it is possible to find in literature more advanced plate theories, which can take into account some of these effects [11, 21, 22].

the generalized plasticity plate model. The latter shows a performance which represents a better approximation of the real three dimensional response if compared to the performance of the classical plasticity plate model.

2   BASIC FRAMEWORK

We present the basic framework for the paper, which is mainly based on an infinitesimal kinematic thick plate theory and an associative flow rule for the evolutionary plastic problem. Early developments of a thick plate theory, which include both bending deformation and the primary effects of transverse shear deformation, are commonly attributed to Reissner [23] and Mindlin [16] and the theory presented here is a simplification of those originally proposed.

Geometry and load

With the term *plate* we refer to a flat slender body, occupying the domain:

$$\Omega = \left\{ (x,y,z) \in \mathcal{R}^3 \mid z \in \left[-\frac{t}{2}, +\frac{t}{2} \right], (x,y) \in \mathcal{A} \subset \mathcal{R}^2 \right\}$$

where the plane $z = 0$ coincides with the mid-surface of the undeformed plate and the transverse dimension, or *thickness t*, is small compared to the other two dimensions.

Furthermore, the loading is restricted to be applied only in the direction normal to the mid-surface.

Kinematics

Limiting the discussion to the realm of infinitesimal kinematics, we assume the following displacement fields:

$$
\begin{aligned}
u(x,y,z) &= \quad z\theta_y(x,y) \\
v(x,y,z) &= -\ z\theta_x(x,y) \\
w(x,y,z) &= \quad w(x,y)
\end{aligned}
$$

(2.1)

where u, v and w are the displacements along the x, y and z axes, respectively, and θ_x and θ_y are the rotations of the transverse line elements about

the x and y axes. Accordingly, a straight line element, normal to the plate mid-surface in the undeformed configuration, remains straight, but not necessarily normal to the deformed mid-surface, allowing for transverse shear deformations. As a direct consequence of equation 2.1, we may assume as a (generalized) *displacement* the vector **u** with components:

$$\mathbf{u} = \left\{ \begin{array}{c} w \\ \theta_x \\ \theta_y \end{array} \right\} = \left\{ \begin{array}{c} w \\ \Theta \end{array} \right\}$$

The basic kinematic ingredients are the curvature and the shear strain, **K** and **Γ**, defined as:

$$\mathbf{K} = \left\{ \begin{array}{c} \kappa_{xx} \\ \kappa_{yy} \\ \kappa_{xy} \end{array} \right\} = \left\{ \begin{array}{c} \theta_{y,x} \\ -\theta_{x,y} \\ \theta_{y,y} - \theta_{x,x} \end{array} \right\}$$

$$\mathbf{\Gamma} = \left\{ \begin{array}{c} \gamma_{xz} \\ \gamma_{yz} \end{array} \right\} = \left\{ \begin{array}{c} \theta_y + w_{,x} \\ -\theta_x + w_{,y} \end{array} \right\}$$

which can be collected in a (generalized) *strain* **E**, defined as:

$$\mathbf{E} = \left\{ \begin{array}{c} \mathbf{K} \\ \mathbf{\Gamma} \end{array} \right\}$$

Note that:

$$\mathbf{\Gamma} = [\mathbf{e}\Theta + \nabla w]$$

where:

$$\mathbf{e} = \left[\begin{array}{cc} 0 & -1 \\ 1 & 0 \end{array} \right]$$

is an alternating matrix and that we may distinguish between in-plane bending strains (ϵ_x, ϵ_y, γ_{xy}) and transverse shear strains (γ_{xz}, γ_{yz}). In the thin plate theory the transverse shear strains are assumed to be zero, thus providing constraint equations which allow one to express θ_x and θ_y as derivatives of the transverse displacement w. Conversely, in the thick plate theory we allow for non-zero shear deformations.

Stresses and stress resultants

As a consequence of the predominance of the behavior associated with the in-plane two dimensions, we may assume the normal stress in the z direction to be negligible compared to the other stresses; hence, we set:

$$\sigma_z = 0$$

Although this position is inconsistent with a general three-dimensional theory and is not present in the work by Reissner (where σ_z varies through the thickness), we may also adopt it since it does not influence the development of a viable finite element formulation.

Consistent with the strain behavior, we may distinguish between in-plane stresses $(\sigma_x, \sigma_y, \tau_{xy})$ and transverse shears (τ_{xz}, τ_{yz}). Their integration through the thickness defines the stress resultants per unit length:

$$M_x = \int_{-\frac{t}{2}}^{\frac{t}{2}} \sigma_x z \, dz \quad , \quad M_y = \int_{-\frac{t}{2}}^{\frac{t}{2}} \sigma_y z \, dz \quad , \quad M_{xy} = \int_{-\frac{t}{2}}^{\frac{t}{2}} \tau_{xy} z \, dz$$

$$Q_x = \int_{-\frac{t}{2}}^{\frac{t}{2}} \tau_{xz} \, dz \quad , \quad Q_y = \int_{-\frac{t}{2}}^{\frac{t}{2}} \tau_{yz} \, dz$$

For notational convenience, we collect the resultants in a (generalized) *stress* **S**:

$$\mathbf{S} = \left\{ \begin{array}{c} \mathbf{M} \\ \mathbf{Q} \end{array} \right\}$$

where:

$$\mathbf{M} = \left\{ \begin{array}{c} M_x \\ M_y \\ M_{xy} \end{array} \right\} \quad , \quad \mathbf{Q} = \left\{ \begin{array}{c} Q_x \\ Q_y \end{array} \right\}$$

Constitutive relation

We now present our definition for an inelastic plate and how we may treat it within an internal variable plasticity theory. For a complete discussion of the internal variable plasticity theory within a three dimensional framework see Lubliner [12].

An *inelastic plate* is one in which the strain **E** is determined by the stress **S** and some additional *internal* or *hidden* variables. We assume that the

inelastic behavior can be treated within the framework of a general plasticity plate theory, as described in References [3, 4, 13]. Accordingly, there exists a continuous *yield function f*, which separates the *elastic* region (for which $f < 0$ and no inelastic effects are present) from the *plastic* region (for which $f \geq 0$ and inelastic deformations occur); furthermore, there exists a continuous *limit function F*, which delimits the domain of all admissible stress states (a stress is admissible only if $F \leq 0$) [2]. In our analysis, we do not require that the limit function F and the yield function f coincide.

Confining the discussion to a small deformation regime, at any time t [3] the strain $\mathbf{E}$ may be additively decomposed into an elastic and a plastic part, $\mathbf{E}^e$ and $\mathbf{E}^p$ respectively:

(2.2)
$$\mathbf{E} = \mathbf{E}^e + \mathbf{E}^p$$

which can be rewritten as:

$$\mathbf{E} = \left\{ \begin{array}{c} \mathbf{K} \\ \mathbf{\Gamma} \end{array} \right\} = \left\{ \begin{array}{c} \mathbf{K}^e \\ \mathbf{\Gamma}^e \end{array} \right\} + \left\{ \begin{array}{c} \mathbf{K}^p \\ \mathbf{\Gamma}^p \end{array} \right\}$$

The elastic strain $\mathbf{E}^e$ is a function only of the stress:

(2.3)
$$\mathbf{E}^e = \mathbf{D}^{e^{-1}} \mathbf{S}$$

$\mathbf{D}^e$ being the appropriate elastic stiffness matrix, which is independent of the strain for a linear elastic response.

The internal variables are assumed to be the plastic strain $\mathbf{E}^p$, the back stress $\mathbf{\Xi}$ and the accumulative plastic strain $\bar{E}^p$. The back stress $\mathbf{\Xi}$ represents the location of the center of the yield surface, which may shift as a result of the kinematic hardening mechanism, while $\bar{E}^p$ is an accumulative measure of the plastic strain, used here to model an isotropic hardening mechanism. Clearly, the presence of additional variables requires additional constitutive equations.

Indicating time derivative with a superposed dot and limiting the discussion only to the case of a flow rule associated with the yield function f (or

---

[2]The yield function f and the limit function F are assumed to be defined in stress space, but corresponding surfaces in the strain space can be easily constructed.

[3]To simplify the notation, the dependence of the variables on the time t is not explicitly stated.

briefly an associative flow rule), as well as to a linear kinematic hardening mechanism, the elasto-plastic problem can be formulated as follow:

$$(2.4) \qquad \mathbf{S} = \mathbf{D}^e \mathbf{E}^e = \mathbf{D}^e \left[\mathbf{E} - \mathbf{E}^p \right]$$

$$(2.5) \qquad \mathbf{\Sigma} = \mathbf{S} - \mathbf{\Xi}$$

$$(2.6) \qquad f = f\left(\mathbf{\Sigma}, \bar{E}^p \right)$$

$$(2.7) \qquad \dot{\mathbf{E}}^p = \dot{\gamma} \frac{\partial f}{\partial \mathbf{\Sigma}} = \dot{\gamma} \mathbf{N}$$

$$(2.8) \qquad \dot{\bar{E}}^p = \|\dot{\mathbf{E}}^p\|_{\mathbf{\Lambda}} = \left(\dot{\mathbf{E}}^{pT} \mathbf{\Lambda} \dot{\mathbf{E}}^p \right)^{\frac{1}{2}}$$

$$(2.9) \qquad \dot{\mathbf{\Xi}} = t H_{kin} \mathbf{\Pi} \dot{\mathbf{E}}^p = t H_{kin} \dot{\gamma} \mathbf{\Pi} \mathbf{N}$$

$$(2.10) \qquad F = F\left(\mathbf{\Sigma}, \bar{E}^p, f, \dot{\gamma} \right)$$

$$(2.11) \qquad \dot{\gamma} \geq 0 \ , \ F \leq 0 \ , \ \dot{\gamma} F = 0$$

where:

- Equation 2.4 is the linear elastic relation between the stress $\mathbf{S}$ and the elastic strain $\mathbf{E}^e$, which is also expressed in terms of total and plastic strain using equation 2.2. In particular, the linear elastic relation can be expanded as:

$$\left\{ \begin{array}{c} \mathbf{M} \\ \mathbf{Q} \end{array} \right\} = \left[\begin{array}{cc} \mathbf{D}_b^e & \mathbf{0} \\ \mathbf{0} & \mathbf{D}_s^e \end{array} \right] \left\{ \begin{array}{c} \mathbf{K}^e \\ \mathbf{\Gamma}^e \end{array} \right\} = \left\{ \begin{array}{c} \mathbf{D}_b^e \left(\mathbf{K} - \mathbf{K}^p \right) \\ \mathbf{D}_b^e \left(\mathbf{\Gamma} - \mathbf{\Gamma}^p \right) \end{array} \right\}$$

where for an isotropic homogeneous plate:

$$\mathbf{D}^b = \frac{Et^3}{12(1-\nu^2)} \left[\begin{array}{ccc} 1 & \nu & 0 \\ \nu & 1 & 0 \\ 0 & 0 & \frac{1}{2}(1-\nu) \end{array} \right]$$

$$\mathbf{D}^s = kGt \left[\begin{array}{cc} 1 & 0 \\ 0 & 1 \end{array} \right]$$

with E being the Young 's modulus, ν the Poisson ratio, G the shear modulus. Finally, k is a factor, introduced to correct the inconsistency between the transverse shear strain, which is constant throughout the thickness, and the shear stress, which is not constant; k depends on the plate properties and is often set equal to 5/6 for isotropic homogeneous plates, value that we retain for both the elastic and the plastic response.

- Equation 2.5 is the definition of the *relative* stress Σ. Note that accordingly to the stress and the strain definition, we can define the back stress as:

$$\Xi = \left\{ \begin{array}{c} \Xi_M \\ \Xi_Q \end{array} \right\}$$

such that the relative stress can be rewritten as:

$$\Sigma = \left\{ \begin{array}{c} M - \Xi_M \\ Q - \Xi_Q \end{array} \right\}$$

- Equation 2.6 is the yield function. A dependence on the scalar accumulative measure of the plastic strain, $\bar{E}^p$, is included to model an isotropic hardening mechanism.

- Equation 2.7 is the constitutive equation (flow rule) for the plastic strain, in the framework of associative plasticity. The $\dot{\gamma}$ is a non negative scalar quantity, embodying the plastic rate characteristic of the model and is called the *consistency parameter*, since it is computed requiring the satisfaction of a specific plasticity model. According to the existence of an elastic region, we have:

$$\dot{\gamma} = 0 \quad \text{when} \quad f < 0$$
$$\dot{\gamma} \geq 0 \quad \text{when} \quad f \geq 0$$

- Equation 2.8 is the constitutive equation for the accumulative plastic strain $\bar{E}^p$, where Λ is an appropriate scaling matrix, which accounts for the different dimensions between the components in $\mathbf{E}^p$.

- Equation 2.9 is the linear constitutive equation for the kinematic hardening mechanism, where H_{kin} is a material parameter, with dimension of stress, and Π is an appropriate scaling matrix, which accounts for the different dimensions between the components of Ξ and $\mathbf{E}^p$.

- Equation 2.10 is the limit function, which may explicitly depend on the yield function f and the consistency parameter $\dot{\gamma}$. Observe again that the functions F and f are not required to be the same, although they may coincide for some specific model, such as classical plasticity.

- Equations 2.11 are the Kuhn-Tucker conditions, which reduce the plastic problem to a constrained optimization problem.

3   VARIATIONAL STRUCTURE

We can deduce the appropriate variational form for the inelastic plate from the variational equation of the corresponding elastic problem.

As discussed in Reference [2], the elastic plate field equations can be derived from the following functional Π, based on the minimum potential energy principle for the bending and on the Hu-Washizu principle for the transverse shear energy:

$$\Pi(w, \boldsymbol{\Theta}, \boldsymbol{\Gamma}, \mathbf{Q}) = \frac{1}{2} \int_A \left[\mathbf{K}^T(\boldsymbol{\Theta}) \, \mathbf{D}_b^e \mathbf{K}(\boldsymbol{\Theta}) \right] dA$$
$$+ \frac{1}{2} \int_A \left[\boldsymbol{\Gamma}^T \mathbf{D}_s^e \boldsymbol{\Gamma} \right] dA - \int_A \left[\mathbf{Q}^T(\boldsymbol{\Gamma} - \nabla w - \mathbf{e}\boldsymbol{\Theta}) \right] dA + \Pi_{ext}$$

where Π_{ext} describes the loads and the boundary effects. Taking the variation of Π with respect to $\mathbf{Q}$, we get:

$$(3.1) \qquad \int_A \left[\delta \mathbf{Q}^T(\boldsymbol{\Gamma} - \nabla w - \mathbf{e}\boldsymbol{\Theta}) \right] dA = 0$$

which can be interpreted as a constraint. Within a finite element setting, we may choose to approximate the $\boldsymbol{\Gamma}$ and $\mathbf{Q}$ fields only in terms of degrees of freedom local to each element (as for example in the case of piecewise constant fields); accordingly, equation 3.1 can be solved in a integral (weak) sense locally to each element [4], rising an expression of the form:

$$(3.2) \qquad \boldsymbol{\Gamma} = \hat{\boldsymbol{\Gamma}}(w, \boldsymbol{\Theta})$$

Using this version of the constraint equation, the functional Π can be reduced to the following one:

$$\Pi_1(w, \boldsymbol{\Theta}) = \frac{1}{2} \int_A \left[\mathbf{K}^T(\boldsymbol{\Theta}) \, \mathbf{D}_b^e \mathbf{K}(\boldsymbol{\Theta}) \right] dA + \frac{1}{2} \int_A \left[\hat{\boldsymbol{\Gamma}}^T \mathbf{D}_s^e \hat{\boldsymbol{\Gamma}} \right] dA + \Pi_{ext}$$

Taking the variation of Π_1, we finally obtain:

$$\delta \Pi_1 = \int_A \left[\delta \mathbf{K}^T \mathbf{D}_b^e \mathbf{K} \right] dA + \int_A \left[\delta \hat{\boldsymbol{\Gamma}}^T \mathbf{D}_s^e \hat{\boldsymbol{\Gamma}} \right] dA + \delta \Pi_{ext}$$

or:

$$\delta \Pi_1 = \int_A \left[\delta \mathbf{K}^T \mathbf{M} \right] dA + \int_A \left[\delta \hat{\boldsymbol{\Gamma}}^T \mathbf{Q} \right] dA + \delta \Pi_{ext}$$

---

[4] For a more detailed discussion of this issue, see again Reference [2].

The appropriate variational equation for the corresponding elasto-plastic plate problem can be deduced from this last relation, where we recall that now:

$$\mathbf{M} = \mathbf{D}_b^e \left(\mathbf{K} - \mathbf{K}^p \right)$$
$$\mathbf{Q} = \mathbf{D}_s^e \left(\hat{\mathbf{\Gamma}} - \mathbf{\Gamma}^p \right)$$

In the following we assume to be understood that the $\mathbf{\Gamma}$ field is computed throughout relation 3.2; hence, to simplify the notation we omit to indicate the hat over $\mathbf{\Gamma}$.

4   CONTINUOUS-TIME MODEL

In Section 2 we presented the equations governing our elasto-plastic plate. The only missing ingredients are the yield and the limit functions, which are presented and discussed now.

Yield function

The yield function f is:

(4.1) $$f = \|\mathbf{\Sigma}\|_A - R$$

with:

$$\|\mathbf{\Sigma}\|_A = \left[\mathbf{\Sigma}^T \mathbf{A} \, \mathbf{\Sigma} \right]^{\frac{1}{2}}$$
$$R = t \left(\sigma_y + H_{iso} \bar{E}^p \right)$$

where σ_y and H_{iso} are material parameters with dimension of stress; in particular σ_y is the material uniaxial initial yielding, while H_{iso} is used to model an isotropic hardening mechanism. The matrix $\mathbf{A}$ is introduced to account for the different dimensions between the components in $\mathbf{\Sigma}$ and is defined as:

$$\mathbf{A} = \frac{9}{4} \begin{bmatrix} \dfrac{16}{t^2}\mathbf{P} & \mathbf{0} \\ \mathbf{0} & 3\mathbf{I}_2 \end{bmatrix}$$

with:

$$\mathbf{P} = \frac{1}{2} \begin{bmatrix} 2 & -1 & 0 \\ -1 & 2 & 0 \\ 0 & 0 & 6 \end{bmatrix}$$

$\mathbf{I}_n$ being the $n \times n$ identity matrix. Note that:

$$\frac{\partial f}{\partial \Sigma} = \frac{\mathbf{A}\Sigma}{\|\Sigma\|_A} = \mathbf{N}$$

and $\mathbf{N}$ is not a unit vector. Assuming no kinematic hardening and expanding equation 4.1, we get:

$$(4.2) \qquad f = \frac{3}{2} \left[\frac{16}{t^2} \left(M_x^2 + M_y^2 - M_x M_y + 3M_{xy} \right) + 3 \left(Q_x^2 + Q_y^2 \right) \right]^{\frac{1}{2}}$$
$$- t \left(\sigma_y + H_{iso} \bar{E}^p \right)$$

It is interesting to observe that if the plate theory is obtained from a three dimensional theory, by integrating the field equations through the thickness, then equation 4.2 can be obtained from the three dimensional von Mises yield function through some manipulations and simplifying assumptions. For this approach we may refer to several papers available in the literature, such as Reference [9, 24, 25]. However, if the simpler and sound *direct approach* to the plate problem is adopted, as discussed in Naghdi [17] and in Green and Naghdi [5, 6], then equation 4.2 can be interpreted as a function of the basic stress quantities and therefore perfectly valid.

From equation 4.2 setting $f = 0$ and dividing by $\sigma_y t$, we obtain a yield condition similar to the one adopted in other works [8, 19, 20, 28]. However we require that the (initial) yielding of the plate occurs at the initial yielding of the cross section of the body, while in the classical plasticity theories the yielding of the plate occurs when the cross section of the body if fully plastic. Moreover, note that the particular form proposed here for f has the advantage of having a normal vector $\mathbf{N} = \partial f / \partial \Sigma$ with the same dimensions as the plastic strain $\mathbf{E}^p$; accordingly, from equation 2.7, we may conclude that the consistency parameter $\dot{\gamma}$ is non-dimensional. This result is desirable for a correct definition of the accumulative plastic strain $\bar{E}^p$. In our analysis we use:

$$\Lambda = \mathbf{A}^{-1}$$

such that:

$$\dot{E}^p = \dot{\gamma}$$

which seems an appropriate result, not obtainable unless $\dot{\gamma}$ is non-dimensional. We also choose:

$$\mathbf{\Pi} = \mathbf{A}^{-1}$$

such that:

$$\dot{\mathbf{\Xi}} = t H_{kin} \dot{\gamma} \mathbf{A}^{-1} \mathbf{N}$$

again giving a dimensional correct relation. Moreover, note that f has dimension of force/length, while the material parameters σ_y, H_{iso} and H_{kin} have all dimension of stress.

Limit function

As limit function for the generalized plasticity plate model, we extend the one presented in References [3, 4, 14]:

$$F = h(f) \frac{d}{dt} [\|\Sigma\|_A] - \dot{\gamma}$$

where h is a non-linear function of the yield function f, defined as:

$$h(f) = \frac{f}{\delta(t\beta - f) + H}$$

with β and δ being two positive constants and $H = t(H_{iso} + H_{kin})$. The parameter β is a scalar measure of the distance between the asymptotic and the current radius of the yield function R and it can be interpreted as a mechanism to model the behavior of the plate from the initial yielding of the section to the fully plastic condition. The parameter δ measures the speed of the model in approaching the asymptotic behavior (see figures 1 and 2).

Other features of the generalized plasticity model are:

- after initial yielding, it shows a smooth transition before reaching an asymptotic value for the stress. The asymptote is horizontal for zero hardening, is not horizontal for non-zero hardening.

- the elasto-plastic stress-strain curve is continuous with its first derivative at the transition point between the elastic and the plastic behavior.

- if unloaded from the plastic range, upon reloading, it renews plasticity before the attainment of the stress where unloading began.

This last feature is unique to the generalized plasticity model and the way in which the model renews plasticity may be easily modified to take into account the behavior of the real materials. For example, if repeated unloading-loading occurs, without plastic deformation in the reverse direction, for each new loading action an increased value of δ can be progressively used. Depending on the material simulated, special updating formulas may be used. Note that no modification to a linearization algorithm should be made since the parameter δ is kept constant during each loading action. Consequently, stress-strain curves of the type represented in figure 3 can be produced; for more discussion relative to this point, see Reference [3].

From an algorithmic point of view, the generalized plasticity model does not present any extra complication compared to a classical plasticity plate model.

5   DISCRETE-TIME MODEL

We now present a discrete time analysis for the elasto-plastic plate problem, paying particular attention to an implementation of the model within a return map algorithm. The form of the elasto-plastic tangent matrix consistent with the discrete model is also addressed.

5.1   Discrete equations and integration algorithm

From a computational standpoint we treat the non-linear behavior of a plate as a *strain driven* problem, since in a finite element implementation the stress history is computed from the strain history by an integration technique, such as a return mapping algorithm. Accordingly, we introduce a discrete counterpart of the equations and review the integration algorithm.

Let $[0, T] \subset \mathcal{R}$ be the time interval of interest and consider two time values within it, say t_n and $t_{n+1} > t_n$, such that t_{n+1} is the first value of interest after t_n. To minimize the appearance of subscripts (to make the equations more readable), we introduce the convention:

$$\mathbf{C}_n = \mathbf{C}(t_n) \ , \quad \mathbf{C} = \mathbf{C}(t_{n+1})$$

where $\mathbf{C}$ is any generic quantity. Accordingly, in the discrete time setting the subscript n indicates a quantity evaluated at time t_n, while no subscript indicates a quantity evaluated at time t_{n+1}.

We assume that the solution is known at time t_n and given by the state:

$$\{\mathbf{S}_n, \mathbf{E}_n, \mathbf{E}_n^p, \bar{E}_n^p, \Xi_n\}$$

We wish to compute the solution at time t_{n+1}, given the total strain $\mathbf{E}$. Using a backward Euler integration formula for the plastic strain, the accumulative plastic strain and the back stress rate equations, we obtain:

$$
\begin{aligned}
\mathbf{E}^p &= \mathbf{E}_n^p + \lambda\,\mathbf{N} \\
\bar{E}^p &= \bar{E}_n^p + \lambda \\
\Xi &= \Xi_n + t H_{kin}\lambda \mathbf{A}^{-1}\mathbf{N}
\end{aligned}
$$

where:

$$\lambda = \int_{t_n}^{t_{n+1}} \dot{\gamma}\,dt$$

is the discrete consistency parameter. The consistency parameters is an unknown quantity and is computed by means of an integration algorithm, such as a return mapping procedure. Initially suggested by Maenchen and Sack [15] and Wilkins [31], the return mapping algorithm provides an efficient and robust integration scheme, based on a discrete enforcement of the model. It belongs to the family of elastic-predictor plastic-corrector algorithms and, hence, is a two part algorithm. In the first part, a purely elastic *trial state* is computed; in the second, if the trial state violates the constitutive equations, a correction is computed using the trial state as initial condition and applied such that the final state is fully consistent with the discrete model. The algorithm has been widely studied [3, 18, 27, 29] as has its stability [10, 26]. Recalling that the incremental elasto-plastic initial value problem formulated as a constrained convex minimization problem is equivalent to the classical *maximum plastic dissipation* postulate, the return mapping algorithm can be shown to be equivalent to a closest point projection of the trial state onto the limit surface $F = 0$. Additional discussion of the algorithm and its theoretical implication can be found in Reference [27].

We now discuss the two steps of the algorithm in more detail.

- *Trial state*: we assume that in the interval $[t_n, t_{n+1}]$ no plastic deformation occurs (i.e. $\mathbf{E}^p = \mathbf{E}^p_n$). Accordingly, as trial values we have:

$$
\begin{aligned}
\lambda^{TR} &= 0 \\
\mathbf{E}^{p,TR} &= \mathbf{E}^p_n \\
\bar{E}^{p,TR} &= \bar{E}^p_n \\
\Xi^{TR} &= \Xi_n \\
\mathbf{S}^{TR} &= \mathbf{D}^e\left[\mathbf{E} - \mathbf{E}^{p,TR}\right] = \mathbf{D}^e\left[\mathbf{E} - \mathbf{E}^p_n\right] \\
\Sigma^{TR} &= \mathbf{S}^{TR} - \Xi^{TR} = \mathbf{S}^{TR} - \Xi_n
\end{aligned}
$$

  If the elastic trial state is admissible, i.e. it does not violate the limit equation F, then it represents the new solution at t_{n+1} and the second part of the algorithm is skipped. If the elastic trial state is not admissible, a correction has to be performed.

- *Plastic correction*: enforcing the full satisfaction of the material model, the consistency parameter λ and the plastic strain $\mathbf{E}^p$ (or equivalently $\mathbf{N}$) may be computed, as shown for a specific model in the next section. The other quantities can be updated in terms of the trial state, λ, $\mathbf{E}^p$ and $\mathbf{N}$ as follow:

$$
\begin{aligned}
\bar{E}^p &= \bar{E}^{p,TR} + \lambda \\
\Xi &= \Xi^{TR} + tH_{kin}\lambda\mathbf{A}^{-1}\mathbf{N} \\
\mathbf{S} &= \mathbf{D}^e\left[\mathbf{E} - \mathbf{E}^p\right] \\
\Sigma &= \mathbf{S} - \Xi
\end{aligned}
$$

5.2   Discrete-time material model

For the specific elasto-plastic model discussed in the paper, the closest point projection of the trial state onto the limit surface $F = 0$ reduces to a radial return projection only if a spectral decomposition algorithm is performed, as discussed for examples in References [8, 28]. However, we believe that the spectral analysis is not an essential ingredient, even from a computational point of view; in fact the computational cost can already be drastically reduced, due to the the sparseness of the matrices involved in the problem.

Hence we solve the closest point projection without performing the eigenanalysis.

For fixed $\mathbf{E}$, solution state at time t_n and trial state at time t_{n+1}, the problem is a function of $\mathbf{E}^p$ and λ and can be cast in the form:

$$\mathbf{R} = \mathbf{E}_n^p + \lambda \mathbf{N} - \mathbf{E}^p = \mathbf{0}$$
$$r = -F(\mathbf{E}^p, \lambda) = 0$$

We solve the system iteratively by a Newton's scheme, as discussed in References [19, 20]; linearizing the problem and using a superscript i for the i-th step of the iteration process, we get:

$$\left\{ \begin{array}{c} \mathbf{R}^{(i+1)} \\ r^{(i+1)} \end{array} \right\} = \left\{ \begin{array}{c} \mathbf{R}^{(i)} \\ r^{(i)} \end{array} \right\} + \left[\begin{array}{cc} \dfrac{\partial \mathbf{R}^{(i)}}{\partial \mathbf{E}^p} & \dfrac{\partial \mathbf{R}^{(i)}}{\partial \lambda} \\ \dfrac{\partial r^{(i)}}{\partial \mathbf{E}^p} & \dfrac{\partial r^{(i)}}{\partial \lambda} \end{array} \right] \left\{ \begin{array}{c} \Delta \mathbf{E}^{p^{(i)}} \\ \Delta \lambda^{(i)} \end{array} \right\} = \left\{ \begin{array}{c} \mathbf{0} \\ 0 \end{array} \right\}$$

which can be solved for $\Delta \mathbf{E}^{p^{(i)}}$ and $\Delta \lambda^{(i)}$:

$$\left\{ \begin{array}{c} \Delta \mathbf{E}^{p^{(i)}} \\ \Delta \lambda^{(i)} \end{array} \right\} = \left[\begin{array}{cc} \mathbf{I}_5 + \lambda^{(i)} \mathbf{B} \mathbf{D}^e & -\mathbf{N} \\ -T_2 \mathbf{C} & -\Omega \end{array} \right]^{-1} \left\{ \begin{array}{c} \mathbf{R}^{(i)} \\ r^{(i)} \end{array} \right\}$$

where:

$$\mathbf{B} = \frac{1}{\|\Sigma\|_A} \left[\mathbf{A} - \mathbf{N} \mathbf{N}^T \right]$$
$$\mathbf{C} = \frac{1}{\|\Sigma\|_A} \Sigma \mathbf{A} \mathbf{D}^e$$

and:

$$T_1 = \delta \lambda + \|\Sigma\|_A - \|\Sigma_n\|_A$$
$$T_2 = T_1 + f$$
$$D = \delta(t\beta - f) + H$$
$$\Omega = D + t H_{iso} T_1$$

Finally, the variables can be updated with the formulas:

$$\left\{ \begin{array}{c} \mathbf{R}^{(i+1)} \\ r^{(i+1)} \end{array} \right\} = \left\{ \begin{array}{c} \mathbf{R}^{(i)} \\ r^{(i)} \end{array} \right\} + \left\{ \begin{array}{c} \Delta \mathbf{E}^{p^{(i)}} \\ \Delta \lambda^{(i)} \end{array} \right\}$$

5.3   Discrete elasto-plastic tangent matrix

We address the form of the elasto-plastic tangent matrix, consistent with the discrete model. The use of a consistent tangent matrix preserves the quadratic convergence of a Newton method, which we adopt in the last section for the incremental solution of a finite element scheme. Linearization of the discrete equations gives:

$$
\begin{aligned}
d\mathbf{E}^p &= d\lambda\,\mathbf{N} + \lambda\,d\mathbf{N} \\
d\bar{E}^p &= d\lambda \\
d\Xi &= tH_{kin}d\lambda\mathbf{A}^{-1}\mathbf{N} + tH_{kin}\lambda\,\mathbf{A}^{-1}d\mathbf{N} \\
d\mathbf{S} &= \mathbf{D}^e d\mathbf{E} - \mathbf{D}^e d\lambda\,\mathbf{N} - \lambda\mathbf{D}^e\,d\mathbf{N}
\end{aligned}
$$

The scalar quantity $d\lambda$ must be computed enforcing the satisfaction of the linearized limit function. We note that:

$$
\begin{aligned}
d\mathbf{N} &= d\left[\frac{\mathbf{A}\Sigma}{\|\Sigma\|_A}\right] \\
&= \frac{1}{\|\Sigma\|_A}\left[\mathbf{A} - \mathbf{N}\mathbf{N}^T\right]d\Sigma \\
&= \mathbf{B}d\Sigma
\end{aligned}
$$

and that:

$$
\begin{aligned}
d\|\Sigma\|_A &= \mathbf{N}^T\mathbf{K}d\mathbf{E} - \mathbf{N}^T\mathbf{K}\mathbf{N}d\lambda \\
df &= \mathbf{N}^T\mathbf{N}d\mathbf{E} - \left(\mathbf{N}^T\mathbf{K}\mathbf{N} + tH_{iso}\right)d\lambda
\end{aligned}
$$

where:

$$
\mathbf{K} = \left[\mathbf{D}^{e^{-1}} + \lambda\mathbf{B}\right]^{-1}
$$

Hence, from the condition:

$$
dF = 0
$$

we get:

$$
d\lambda = U\,\mathbf{N}^T\mathbf{K}\,d\mathbf{E}
$$

where U is a scalar factor, given by:

$$U = \frac{T_1}{T_1 \mathbf{N}^T \mathbf{K} \mathbf{N} + T_2 t H_{iso} + D}$$

We can finally reduce the problem to the following two vector equations:

$$\begin{bmatrix} \mathbf{I}_5 & \lambda \mathbf{K} \mathbf{B} \\ -t H_{kin} \lambda \mathbf{B} & [\mathbf{A} + t H_{kin} \lambda \mathbf{B}] \end{bmatrix} \begin{Bmatrix} d\mathbf{S} \\ d\Xi \end{Bmatrix} = \begin{Bmatrix} \mathbf{K} - U \mathbf{K} \mathbf{N} \mathbf{N}^T \mathbf{K} \\ t H_{kin} \mathbf{N} \mathbf{N}^T \mathbf{K} \end{Bmatrix} d\mathbf{E}$$

which requires the inversion of the matrix on the left hand side for its solution, returning a symmetric tangent at the end. In particular, for the case of no kinematic hardening, the consistent tangent matrix may be computed without performing any inversion:

$$d\mathbf{S} = \left[\mathbf{K} - U \hat{\mathbf{N}} \hat{\mathbf{N}}^T \right] d\mathbf{E}$$

where:

$$\hat{\mathbf{N}} = \mathbf{K} \mathbf{N}$$

Note that the form of the consistent tangent matrix strongly recall the one obtainable from a three dimensional theory, as discussed in Reference [3].

6   FINITE ELEMENT APPROXIMATION

We now present a simple triangular finite element, developed within the thick plate theory discussed in Section 2.

6.1   A triangular thick plate finite element

Expressing the shape functions in terms of area coordinates, L_i, as described in Reference [32], the triangular region occupied by each element may be expressed as:

$$\mathbf{x} = \sum_{i=1}^{3} L_i \hat{\mathbf{x}}_i$$

where $0 \leq L_i \leq 1$, $L_1 + L_2 + L_3 = 1$, $\mathbf{x} = \{x, y\}^T$ and where $\hat{\mathbf{x}}_i = \{\hat{x}_i, \hat{y}_i\}^T$ are the nodal coordinates [5].

The element has three external (global) displacement degrees-of-freedom at each vertex i: the transverse displacement $\hat{w}_i$ and the two components of the rotation along the x-y coordinate axes, $\hat{\theta}_{ix}$ and $\hat{\theta}_{iy}$, respectively. In addition, to meet the mixed patch test requirements and to improve the interpolation, two internal rotational degrees-of-freedom, $\Delta\hat{\theta}_x$ and $\Delta\hat{\theta}_x$, associated with a cubic bubble function are added, for a total of eleven displacement degrees-of-freedom (see figure 4). Accordingly, the interpolation for the rotational fields is:

$$\Theta = \sum_{i=1}^{3} L_i \hat{\Theta}_i + 27 L_1 L_2 L_3 \Delta\hat{\Theta}$$

where:

$$\hat{\Theta}_i = \left\{ \begin{array}{c} \hat{\theta}_{ix} \\ \hat{\theta}_{iy} \end{array} \right\}$$

$$\Delta\hat{\Theta} = \left\{ \begin{array}{c} \Delta\hat{\theta}_x \\ \Delta\hat{\theta}_x \end{array} \right\}$$

The transverse displacement interpolation is taken as a simple linear function, enhanced by quadratic terms expressed in terms of the normal components of the nodal rotations for each side of the element:

$$w = \sum_{i=1}^{3} L_i \hat{w}_i - \frac{1}{2} \sum_{i=1}^{3} L_i L_j \left(\hat{\theta}_{jn} - \hat{\theta}_{in} \right) l_k$$

where $\hat{\theta}_{jn}$ and $\hat{\theta}_{in}$ are the components of the rotations of nodes j and i in the direction normal to the i-j side. In this last equation the indices i, j, k are a cyclic permutation which may be written compactly as: $j = mod(i, 3) + 1$ and $k = mod(j, 3) + 1$ [6] , while l_k is the length of the side between the nodes i and j and opposite to the node k.

The shear strain and the shear stress are:

$$\mathbf{\Gamma} = \bar{\mathbf{\Gamma}} = \left\{ \begin{array}{c} \bar{\gamma}_x \\ \bar{\gamma}_y \end{array} \right\}$$

---

[5] The indices i, j and k always range in $\{1, 2, 3\}$.

[6] The mod(i,j) is a standard programming remainder function equal to i-(i/j)*j where integer arithmetic is used to compute i/j .

$$\mathbf{Q} = \bar{\mathbf{Q}} = \left\{ \begin{array}{c} \bar{Q}_x \\ \bar{Q}_y \end{array} \right\}$$

where the superposed bar indicates that both fields are constant over each element.

The same element has been tested using a 7-point formula and a 1-point formula for the case of linear elastic material and the results are presented in Reference [1]. In the present work we adopt a three point formula, described in Reference [7]; the location of the integration points is shown in figure 4. It is interesting to observe that:

- in the solution of linear elastic problem the element obtained using the 3-point formula performs slightly better than the one presented in Reference [1].

- due to the symmetric location of the quadrature points and the constant weights [7], the numerical implementation of the element can be optimized to obtain an efficient element; as an example note that, the constraint equation 3.1 may be computed in closed form, except for the contribution of the bubble function.

We finally recall that due to the mixed approach presented in Section 3 and also discussed in References [2] and [3], the reduced quadrature is associated only with the specification of the strain displacement relation and with the constraint equation 3.1, thus not precluding the use of the element with non-linear constitutive models. This is in contrast with the use of reduced quadrature in finite elements based on a displacements approach.

For the results reported in the next section, the finite element load is consistent with the transverse displacement interpolation.

6.2   Global solution and tangent consistent matrix

Assembling the quantities relative to each element (henceforth called local) yields the following (global) non-linear system of equations:

$$(6.1) \qquad \mathop{\mathcal{A}}_{e=1}^{n_{elm}} \left[f_e^{int} \left(\mathbf{u}_e, \Delta \Theta_e \right) - f_e^{ext} \right] = \mathbf{0}$$

$$(6.2) \qquad \mathbf{h} \left(\mathbf{u}_e, \Delta \Theta_e \right) = \mathbf{0} \quad e = 1, 2, \dots n_{elm}$$

where: $\mathcal{A}$ denotes the standard assembly operator, $\mathbf{u}_e$ and $\boldsymbol{\Delta\Theta}_e$ are the external and the internal degrees of freedom relative to the e element, n_{elm} is the total number of elements, f_e^{int} and f_e^{int} are the force vectors, associated with the internal stresses and the external loads respectively. The first set of equations represents the equilibrium of the external degrees of freedom, while the second set of equations represent the equilibrium of the internal degrees of freedom relative to each element. Within each time step the solution of this non-linear system is accomplished by an iterative Newton procedure, based for each iteration i on the following steps:

- recovering of the internal degrees of freedom with an iterative technique such to satisfy equation 6.2 within each element

- solution of the global linearized problem associated with equation 6.1.

Note that the recovering of the internal degrees of freedom is performed by a local iterative technique; in fact for each element e, equation 6.2 involves only quantities relative to the e element, hence it can be solved at the element level.

7   NUMERICAL EXAMPLES

To test the generalized plasticity plate theory we now present some numerical examples, organized as follow:

- Cantilever beam: limit load

- Cantilever beam: cyclic load

- Clamped circular plate: limit load

- Clamped circular plate: cyclic load

- Clamped square plate: limit load

- Clamped square plate: cyclic load

For each problem, we present the results from both three and two dimensional analyses. The three dimensional analysis is performed using a

classical plasticity constitutive model (see for example Reference [29]), and a *mixed* finite element [30]. The two dimensional analyses are performed using a classical plasticity model [19, 20] and the generalized plasticity model, here proposed; moreover they are obtained running the plate element discussed in the previous section. Both finite elements are implemented into the Finite Element Analysis Program (FEAP) [32, 33].

7.1   Cantilever beam: limit load

We analyze a cantilever beam (figure 5) under simple flexure in the y-z plane; the load is applied controlling the curvatures at both ends. The geometrical parameter of the problem are:

$$L = 1 \ , \ \ b = 2 \ , \ \ t = 2$$

with initial yielding stress:

$$\sigma_y = 60$$

Due to the symmetry and asymmetry of the problem, only one fourth of the body is discretized for the three dimensional analysis and in figure 6 the adopted mesh is presented in a deformed configuration. In figure 7 we plot the bending moment versus the curvature ratio, defined as κ_{yy}/κ_Y, κ_Y being the curvature at initial yielding. As expected the moment per unit length at initial yielding is given by $M_Y = 40$, while the ultimate moment M_U is given by:

$$M_U = \frac{3}{2} M_Y = 60$$

This result is due to the progressive diffusion of the plastic flow in the cross section of the beam: hence it is clearly a consequence of the three dimensionality of the problem and related to the motion in the transverse direction.

The cantilever beam is then studied using a two dimensional theory and the adopted mesh is presented in figure 8; using a classical plasticity plate model the usual piecewise linear moment curvature relation is obtained, which is far from the result of the three dimensional analysis (see the piecewise dot-dash curve in figure 10). A better simulation of the real behavior of the cantilever beam can be obtained using the generalized plasticity model, for which we choose $\beta = M_U - M_Y = 20$. First we test the model for different values of δ (figure 9), which shows the reliability and the capacity of the

model. In figure 10 we present the moment-curvature relation for the generalized plasticity model with $\delta = 12$ (continuous line) versus the one obtained from the three-dimensional analysis (dotted line); you can note the good agreement between the two. Moreover, for comparison the curve relative to classical plasticity is also reported (dot-dash line).

7.2   Cantilever beam: cyclic load

We now consider a cantilever beam under cyclic loading conditions. The geometric and the material properties, as well as the finite element meshes, are the same of those adopted for the case of monotonic loading. In figure 11 we present the moment-curvature ratio curve for the two dimensional analyses versus the three dimensional analysis.

7.3   Clamped circular plate: limit load

We analyze a clamped circular plate under a uniform distributed load in the transverse direction. The radius of the plate is $r = 10$, while the thickness is $t = 2$; for all the models, we use the parameters determined in the first analysis (cantilever beam: limit load).

Again, due to the symmetry and asymmetry of the problem, only the top half of a circular sector with angle equal to $5°$ is discretized for the three dimensional analysis and in figure 12 the adopted mesh is presented in a deformed configuration. The two dimensional mesh is shown in figure 13. In figure 14 we plot the transverse distributed load q versus the displacement at the center of the plate for the three-dimensional plasticity model, the classical and generalized two dimensional plasticity models. Again you can note that the generalized plasticity plate model matches the three dimensional response with greater accuracy, then the classical plasticity plate model.

7.4   Clamped circular plate: cyclic load

We now consider the same clamped circular plate under cyclic loading conditions. The geometric and the material properties, as well as the finite element meshes, are the same of those adopted for the case of monotonic loading. In figure 15 we plot the transverse distributed load q versus the

displacement at the center of the plate for the three-dimensional plasticity model, the classical and generalized two dimensional plasticity models.

7.5   Clamped square plate: limit load

We analyze a clamped square plate under a uniform distributed load in the transverse direction. The span of the plate is $L = 20$, while the thickness is $t = 2$; for all the models, we use the parameters determined in the first analysis (cantilever beam: limit load).

Due to the symmetry and asymmetry of the problem, again only the top half of a quarter of the plate is discretized for the three dimensional analysis and in figure 16 the adopted mesh is presented in a deformed configuration. The two dimensional mesh is shown in figure 17. In figure 18 we plot the transverse distributed load q versus the displacement at the center of the plate for the three-dimensional plasticity model, the classical and generalized two dimensional plasticity models. You can note a greater accuracy of the generalized plasticity plate model, compared to classical plasticity plate one.

7.6   Clamped square plate: cyclic load

We now consider the same clamped square plate under cyclic loading conditions. The geometric and the material properties, as well as the finite element meshes, are the same of those adopted for the case of monotonic loading. In figure 15 we plot the transverse distributed load q versus the displacement at the center of the plate for the three-dimensional plasticity model, the classical and generalized two dimensional plasticity models.

CLOSURE

In the present paper we present and discuss the continuous and the discrete time version of a new generalized plasticity plate model, which is able to reproduce some of the three dimensional effects of a non-linear thin body (spreading of inelastic effect in the cross section) within a two dimensional theory. This new plasticity model admits the existence of an (initial) yield function and a limit (final) function, which are not required to coincide. Hence, we choose the (initial) yield function for the plate to reproduce a

uniaxial initial yielding moment of the three dimensional body, while the limit (final) limit function is chosen to reproduce the final plastic moment, in which the cross section is fully plastic.

The numerical examples show that the generalized plasticity model predicts results which agree with those obtained from a three dimensional classical elasto-plastic solution; moreover, they are closer than those obtainable from a classical plasticity plate model. We note that the computational costs and implementation of the two dimensional models are comparable; hence, we may conclude that the proposed generalized plasticity model represents a significant improvement over existing classical plasticity theories.

References

[1] F. Auricchio and R.L. Taylor, *Linked interpolation for Reissner-Mindlin plate elements: Part II: a simple triangle*, International Journal for Numerical Methods in Engineering, to appear.

[2] _____ , *3-node triangular elements based on Reissner-Mindlin plate theory*, Report UCB/SEMM-91/04, Department of Civil Engineering, University of California at Berkeley, 1991.

[3] _____ , *Two material models for cyclic plasticity: non-linear kinematic hardening and generalized plasticity*, Report UCB/SEMM-93/03, Department of Civil Engineering, University of California at Berkeley, 1993.

[4] F. Auricchio, R.L. Taylor, and J. Lubliner, *Application of a return map algorithm to plasticity models*, COMPLAS Computational Plasticity: Fundamentals and Applications (Barcelona) (D.R.J. Owen and E. Onate, eds.), 1992, pp. 2229–2248.

[5] A.E. Green and P.M. Naghdi, *On the derivation of shell theories by direct approach*, Journal of Applied Mechanics **41** (1974), 173–176.

[6] _____ , *A thermomechanical theory of a Cosserat point with application to composite materials*, Quart. J. Mech. Appl. Math. **44** (1991), 335–355.

[7] T.J.R. Hughes, *The finite element method*, Prentice Hall, 1987.

[8] A. Ibrahimbegovic and F. Frey, *An efficient implementation of stress resultant plasticity in analysis of Reissner-Mindlin plates*, International Journal for Numerical Methods in Engineering **36** (1993), 303–320.

[9] G.V. Ivanov, *Approximating the final relationship between the forces and moments of shells under the Mises plasticity condition*, Mekhanika Tverdogo Tela **2** (1967), 74–75.

[10] R.D. Krieg and D.B. Krieg, *Accuracies of numerical solution methods for the elastic-perfectly plastic model*, Journal of Pressure Vessel Technology, Transaction of ASME (1977), 510–515.

[11] K.H. Lo, R.M. Christensen, and E.M. Wu, *A high order theory of plate deformation*, Journal of Applied Mechanics **44** (1977), 663–676.

[12] J. Lubliner, *Plasticity theory*, Macmillan, 1990.

[13] ———, *A simple model of generalized plasticity*, International Journal of Solids and Structures **28** (1991), 769–778.

[14] J. Lubliner, R.L. Taylor, and F. Auricchio, *A new model of generalized plasticity*, International Journal of Solids and Structures, to appear.

[15] G. Maenchen and S. Sack, *The tensor code*, Methods in computational physics (B. Alder, ed.), vol. 3, Academic Press, 1964, pp. 181–210.

[16] R.D. Mindlin, *Influence of rotatory inertia and shear in flexural motion of isotropic, elastic plates*, Journal of Applied Mechanics **18** (1951), 31–38.

[17] P.M. Naghdi, *Finite deformation of elastic rods and shells*, Proc. IUTAM Symposium on Finite Elasticity (Bethlehem PA) (D.E. Carlson and R.T. Shield, eds.), 1982, pp. 47–103.

[18] J.C. Nagtegaal, *On the implementation of inelastic constitutive equations with special reference to large deformation problems*, Computer Methods in Applied Mechanics and Engineering **33** (1982), 469–484.

[19] P. Papadopoulos and R.L. Taylor, *An elasto-plastic analysis of Reissner-Mindlin plates*, Applied Mechanics Review **43** (1990), 540–550.

[20] _____, *An analysis of inelastic Reissner-Mindlin plates*, Finite Elements in Analysis and Design **10** (1991), 221–233.

[21] R. Piltner, *The derivation of a thick and thin plate formulation without ad hoc assumptions*, Journal of Elasticity **29** (1992), 133–173.

[22] _____, *A quadrilateral hybrid-Trefftz plate bending element for the inclusion of warping based on a three-dimensional plate formulation*, International Journal for Numerical Methods in Engineering **33** (1992), 387–408.

[23] E. Reissner, *The effect of transverse shear deformation on the bending of elastic plates*, Journal of Applied Mechanics **12** (1945), 69–76.

[24] M. Robinson, *A comparison of yield surfaces for thin shells*, International Journal of Mechanical Sciences **13** (1971), 345–354.

[25] G.S. Shapiro, *On yield surfaces for ideally plastic shells*, Problems of Continuum Mechanics (1961), 414–418.

[26] J.C. Simo and S. Govindjee, *Non-linear B-stability and symmetry preserving return mapping algorithms for plasticity and visco-plasticity*, International Journal for Numerical Methods in Engineering **31** (1991), 151–176.

[27] J.C. Simo and T.J.R. Hughes, *Elasto-plasticity and visco-plasticity: computational aspects*, Springer-Verlag, 1993, to appear.

[28] J.C. Simo and J.G. Kennedy, *On a stress resultant geometrically exact shell model. Part V. Nonlinear plasticity: formulation and integration algorithms*, Computer Methods in Applied Mechanics and Engineering **96** (1992), 133–171.

[29] J.C. Simo and R.L. Taylor, *Consistent tangent operators for rate-independent elasto-plasticity*, Computer Methods in Applied Mechanics and Engineering **48** (1985), 101–118.

[30] J.C. Simo, R.L. Taylor, and K.S. Pister, *Variational and projection methods for the volume constraint in finite deformation elasto-plasticity*, Computer Methods in Applied Mechanics and Engineering **51** (1985), 177–208.

[31] M.L. Wilkins, *Calculation of elastic plastic flow*, Methods in computational physics (B. Alder, ed.), vol. 3, Academic Press, 1964, pp. 211–263.

[32] O.C. Zienkiewicz and R.L. Taylor, *The finite element method*, fourth ed., vol. I, McGraw Hill, New York, 1989.

[33] _____, *The finite element method*, fourth ed., vol. II, McGraw Hill, New York, 1991.
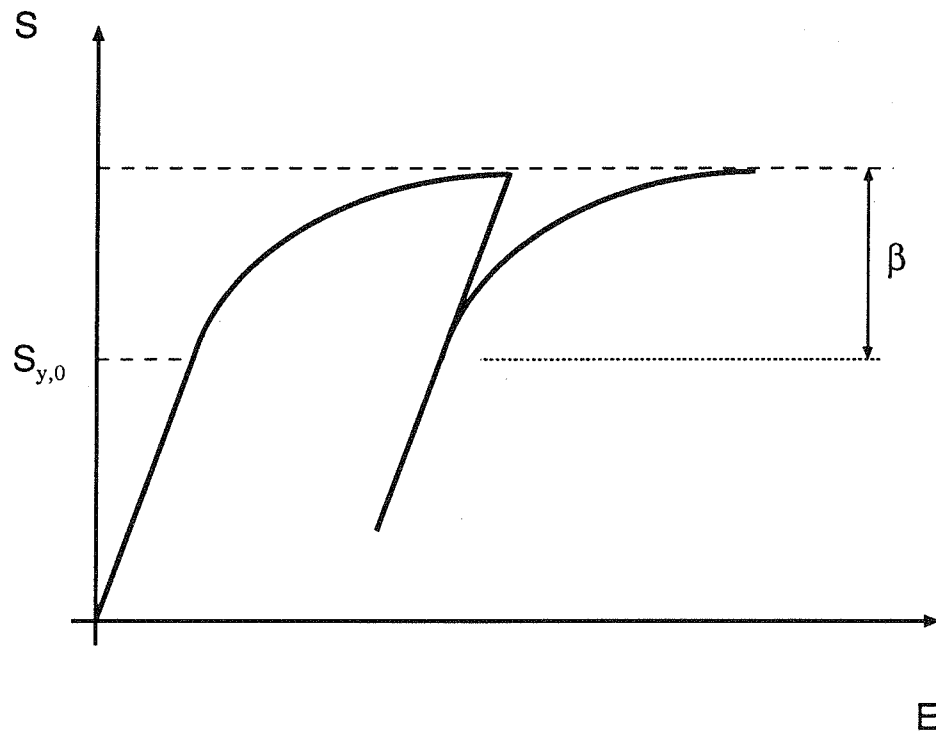
Figure 1: Generalized plasticity model with no hardening. Stress **S** versus strain **E**.
The model reaches an horizontal asymptote and, if unloaded from the plastic range and reloaded before the occurrence of reverse plasticity, it renews plasticity before the attainment of the stress at which the unloading began.
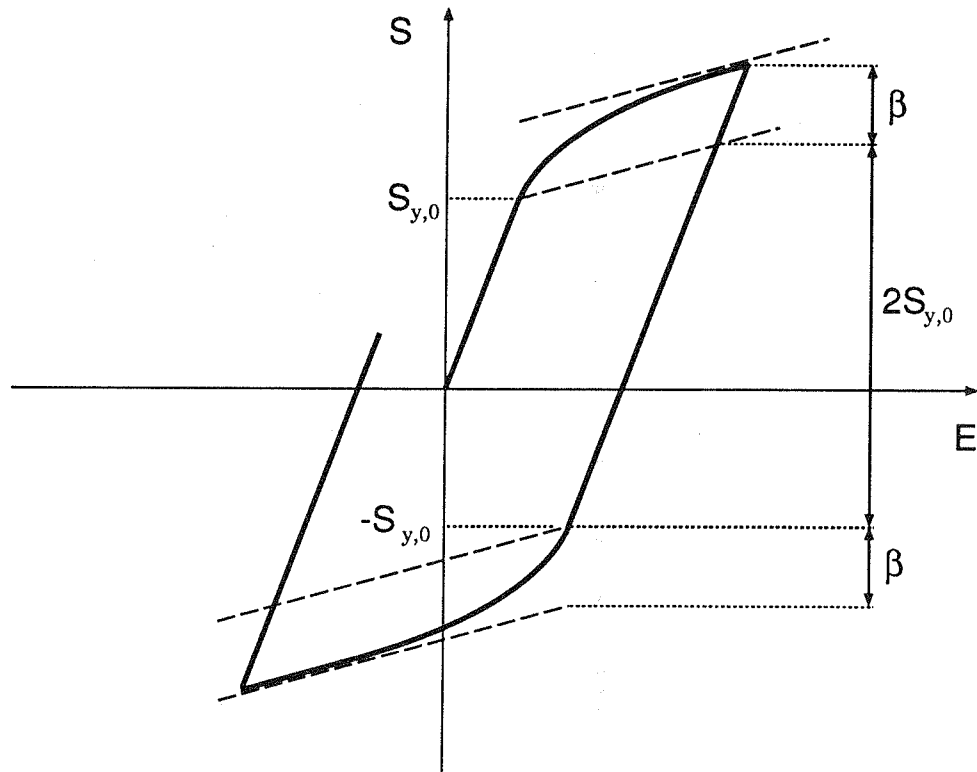
Figure 2: Generalized plasticity model under cyclic loading condition. Stress **S** versus strain **E**.
Zero isotropic hardening, non-zero kinematic hardening.
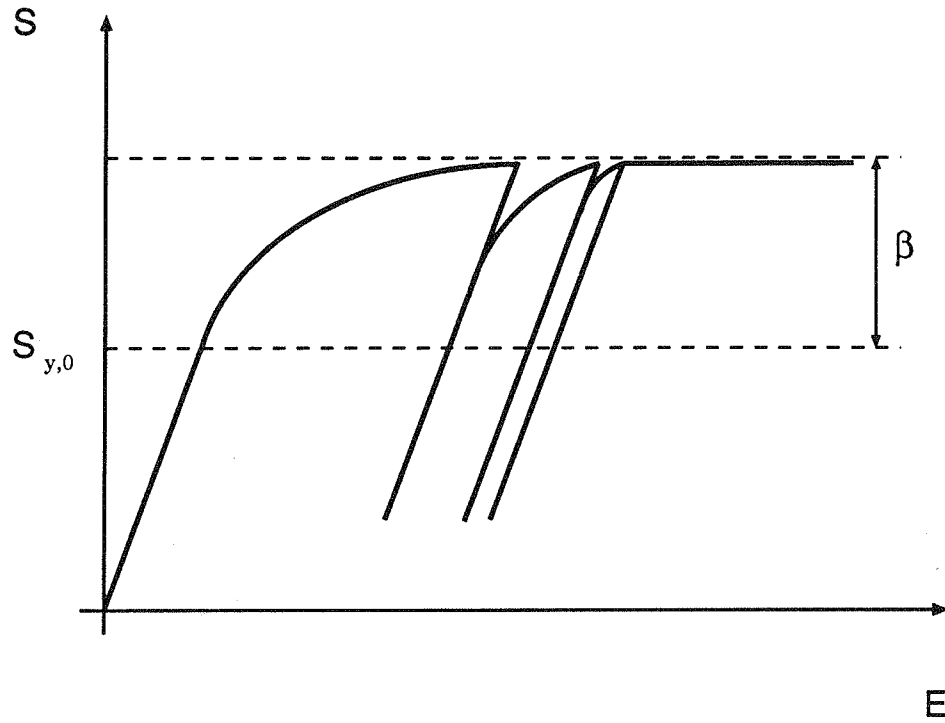
Figure 3: Generalized plasticity model with no hardening and update for the δ parameter. Stress **S** versus strain **E**.
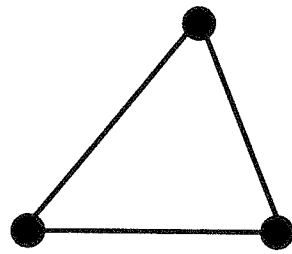
w-parameters
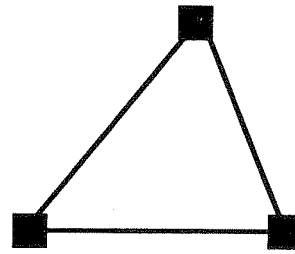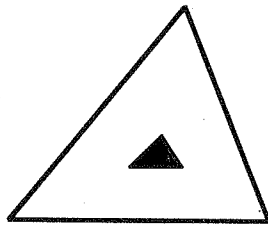
θ-parameters
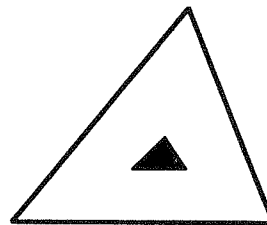
Γ-parameters

Q-parameters
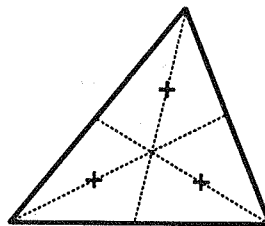
Quadrature points

Figure 4: Degrees of freedom for the triangular thick plate finite element and location of the quadrature points.
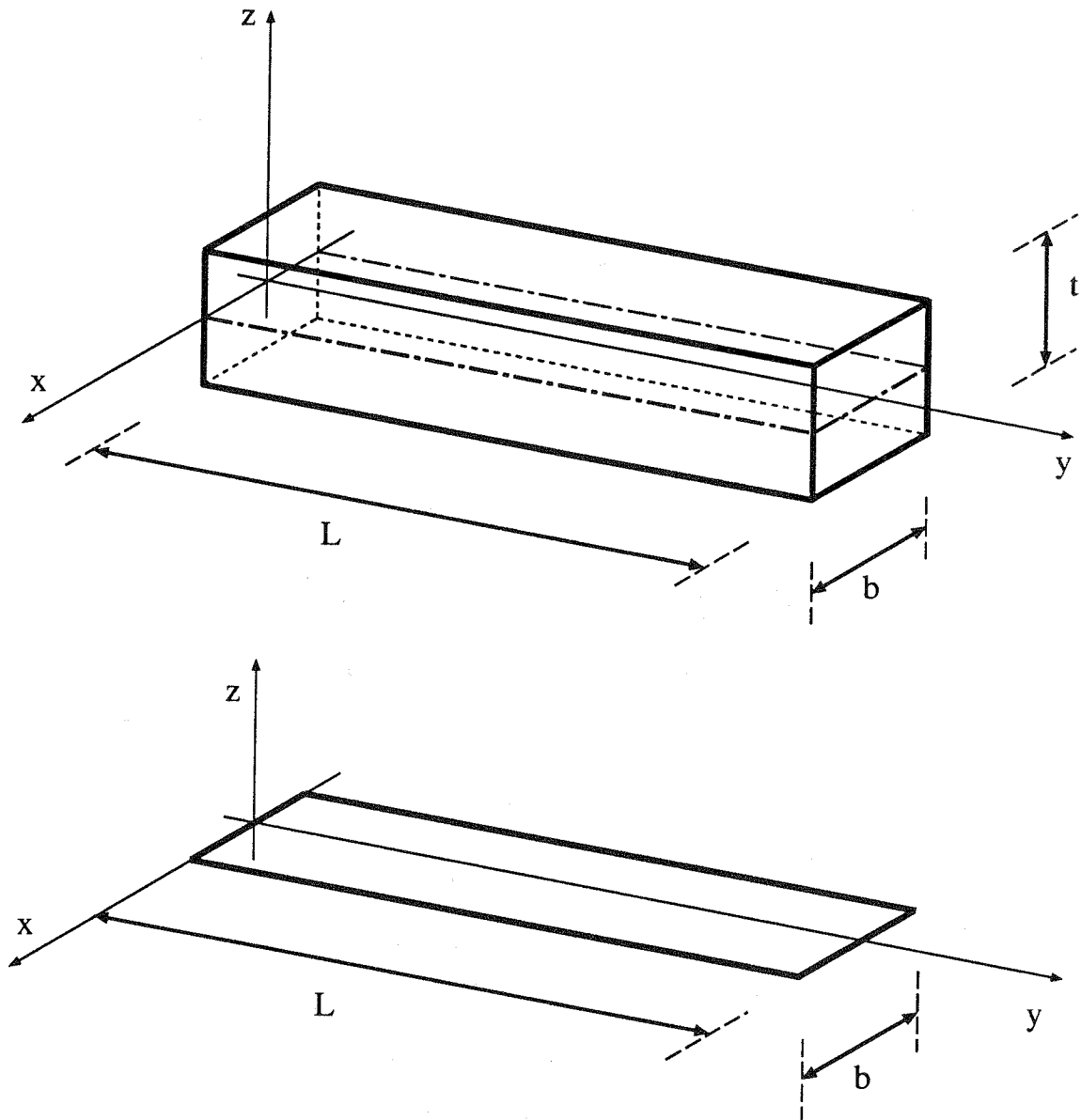
Figure 5: Cantilever beam: three dimensional problem and reduction to two dimension.
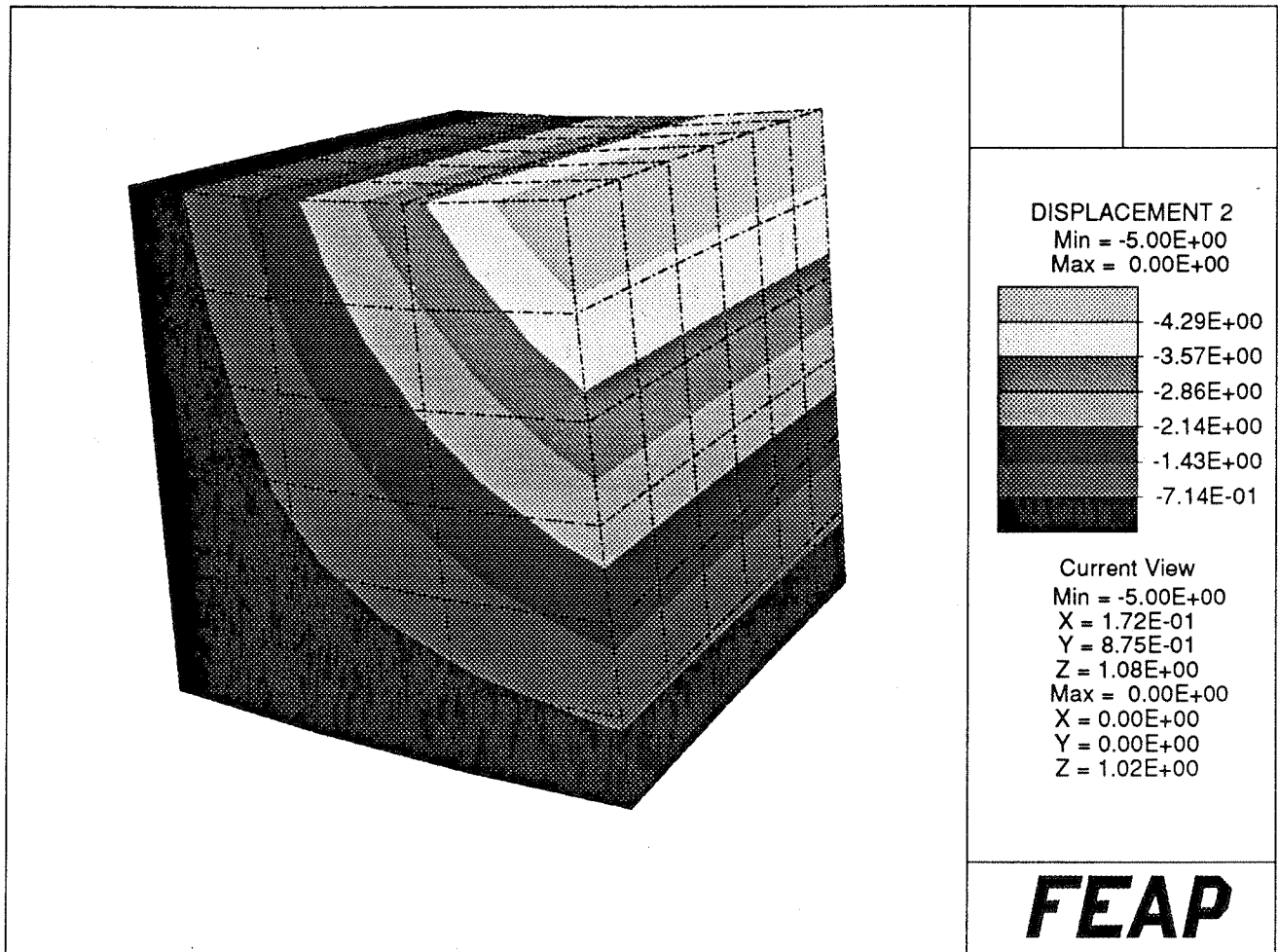
Figure 6: Cantilever beam: three dimensional mesh in a deformed configuration.
The contour lines for the y displacements are also shown.
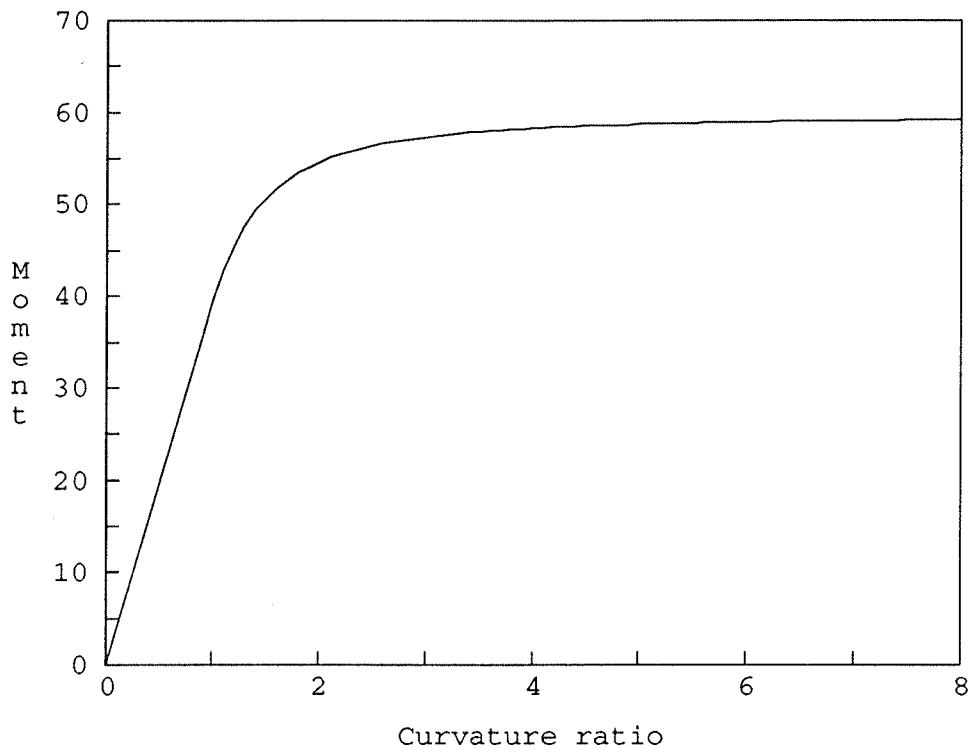
Figure 7: Cantilever beam: limit load. Three dimensional analysis. Bending moment versus curvature ratio.

DISPLACEMENT 3
Min = 0.00E+00
Max = 5.00E+00

7.14E-01
1.43E+00
2.14E+00
2.86E+00
3.57E+00
4.29E+00

Current View
Min = 0.00E+00
X = 0.00E+00
Y = 0.00E+00

Max = 5.00E+00
X = 1.00E+00
Y = 0.00E+00

FEAP
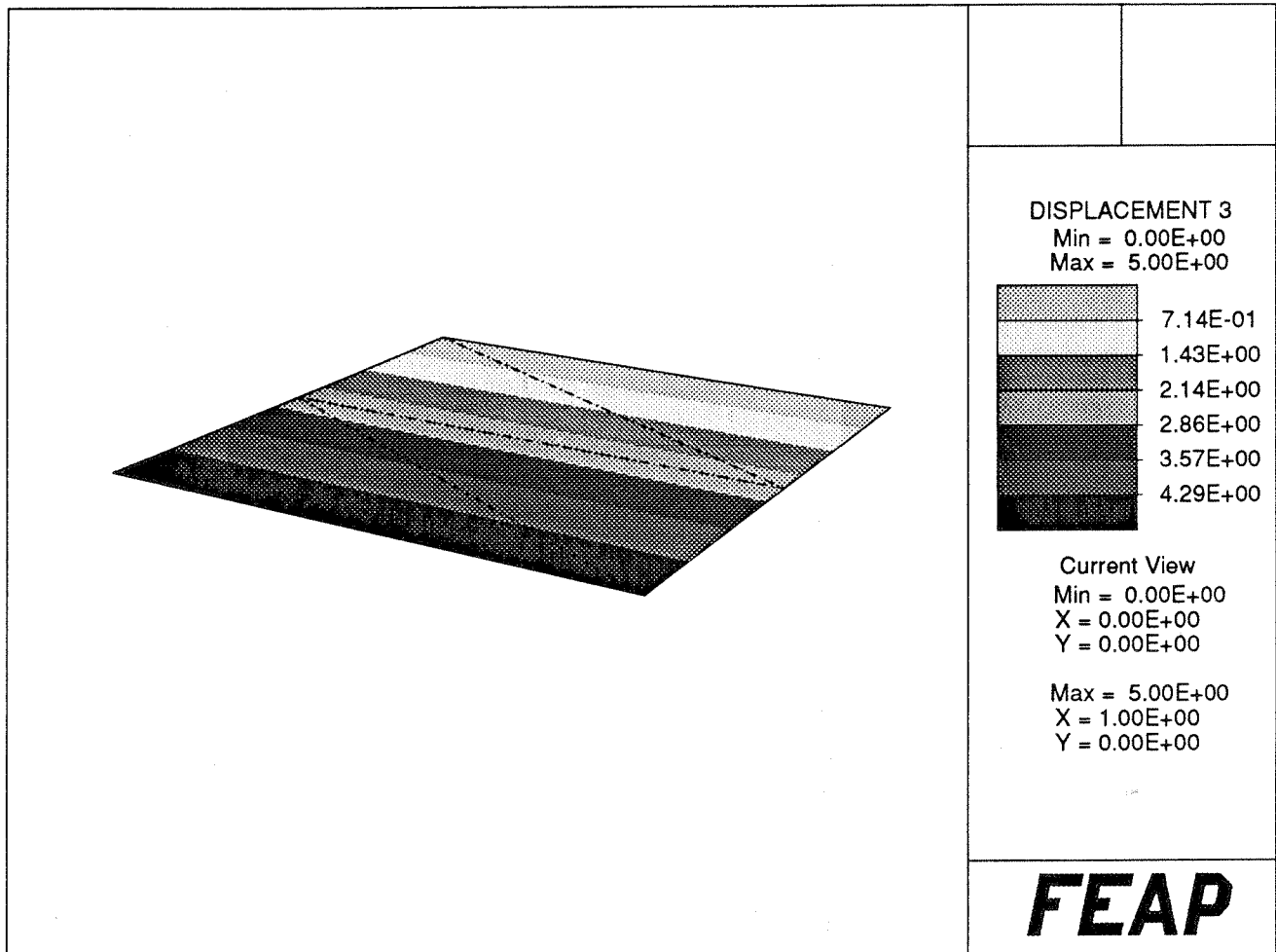
Figure 8: Cantilever beam: two dimensional mesh in the undeformed configuration.
The contour lines for the vertical displacements are also shown.
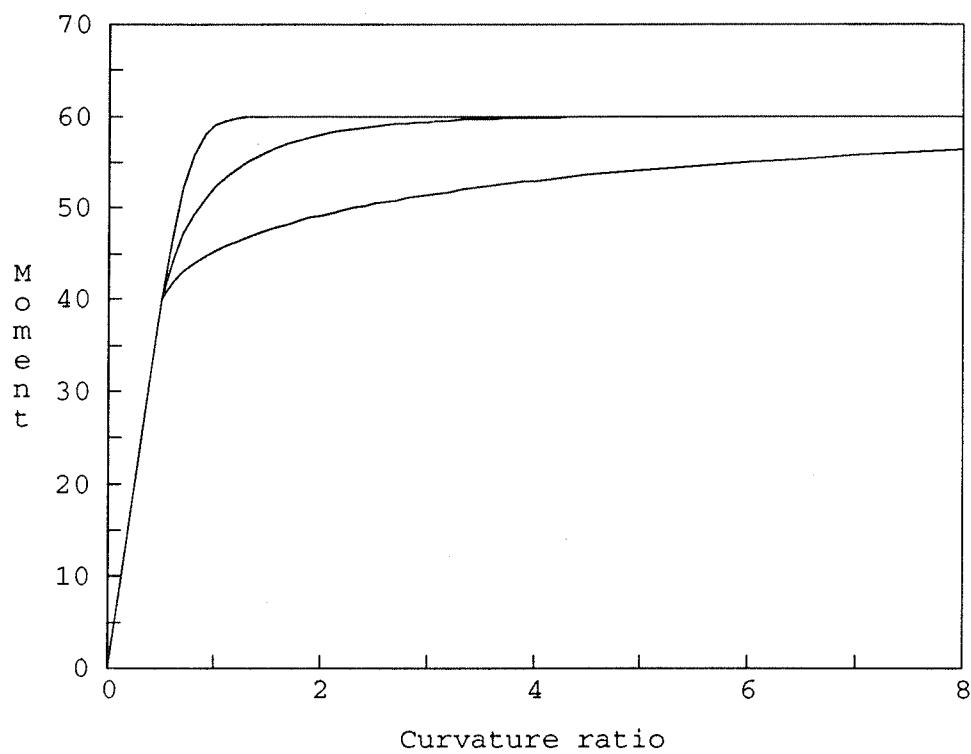
Figure 9: Generalized plasticity model. Moment versus curvature ratio for different values of the parameter δ: $\delta \in \{1, 10, 100\}$
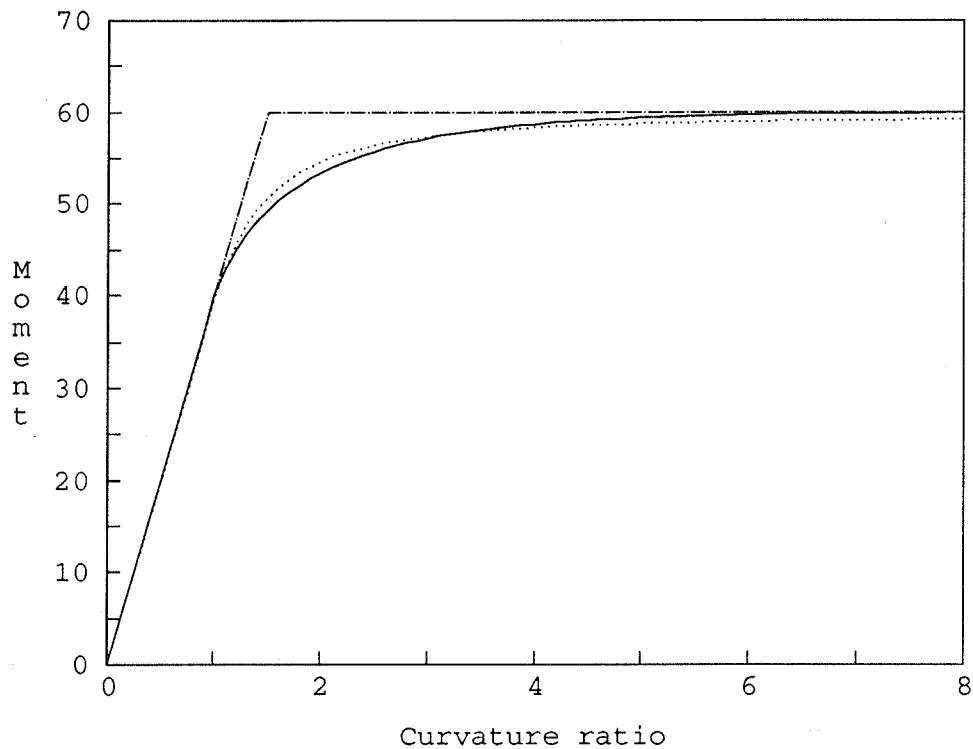
Figure 10: Cantilever beam: limit load. Two dimensional analysis versus three dimensional analysis.
Moment-curvature relation for generalized plasticity plate model (continuous line), classical plasticity plate model (dot-dash line) and three-dimensional classical plasticity model (dotted line).
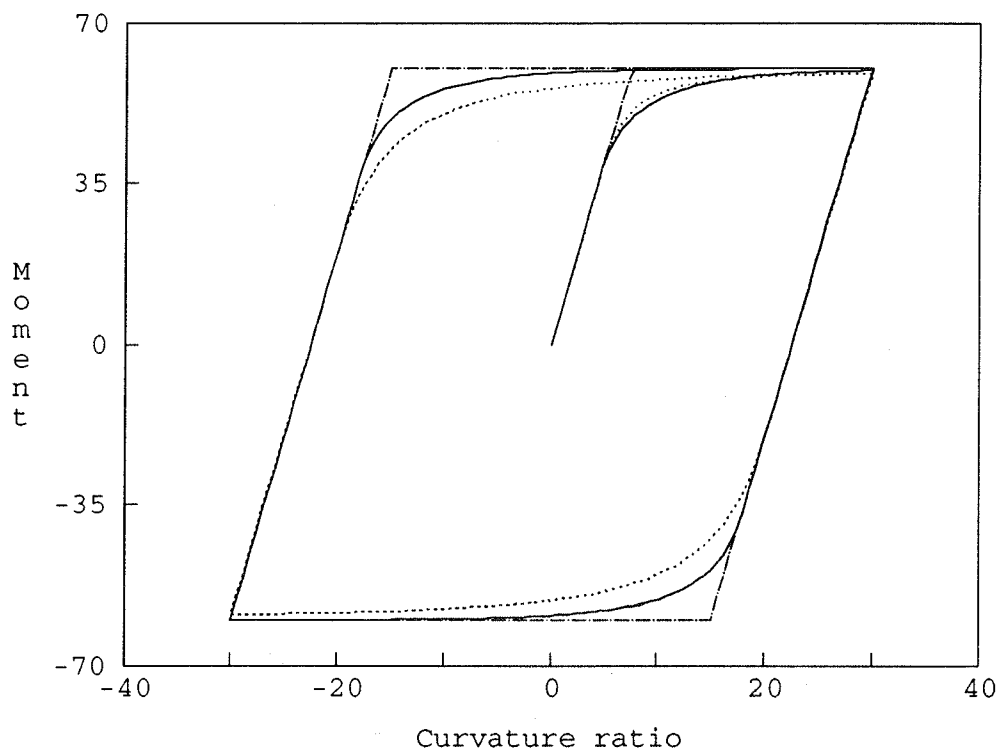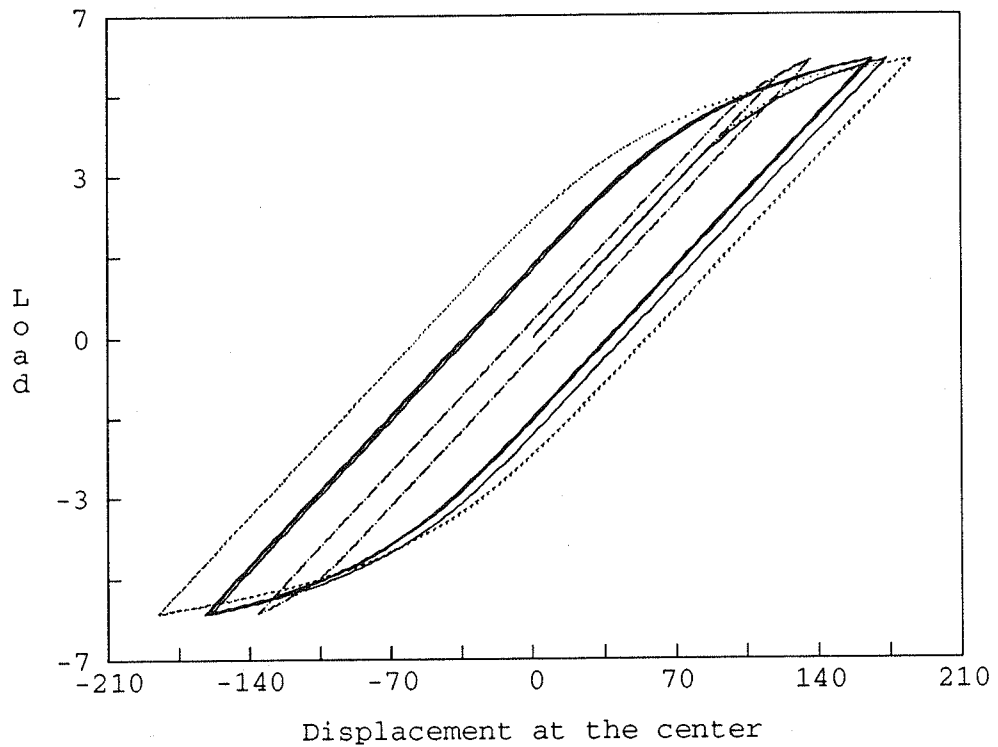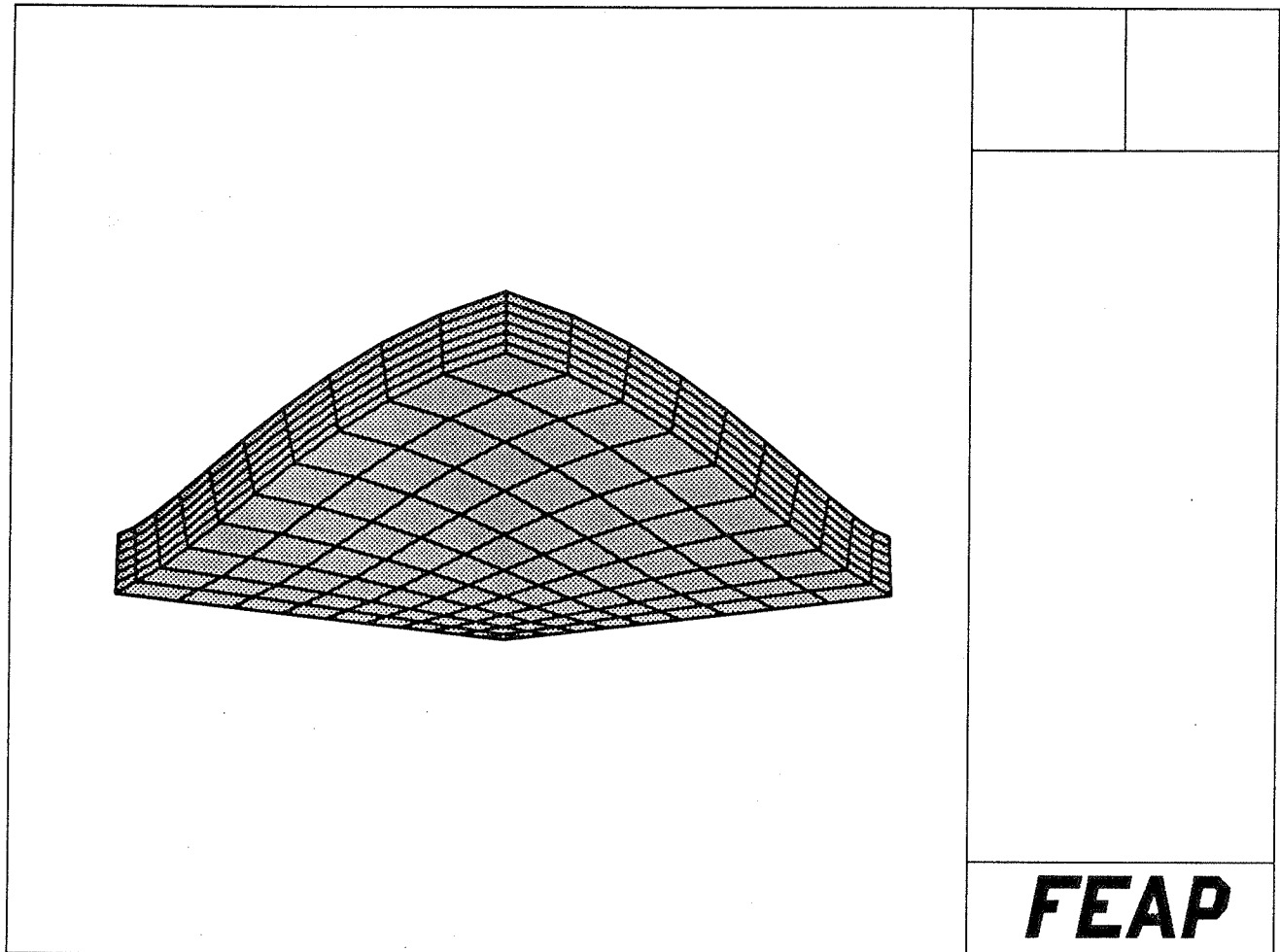
Figure 11: Cantilever beam: cyclic load. Two dimensional analysis versus three dimensional analysis.
Moment-curvature relation for generalized plasticity plate model (continuous line), classical plasticity plate model (dot-dash line) and three-dimensional classical plasticity model (dotted line).
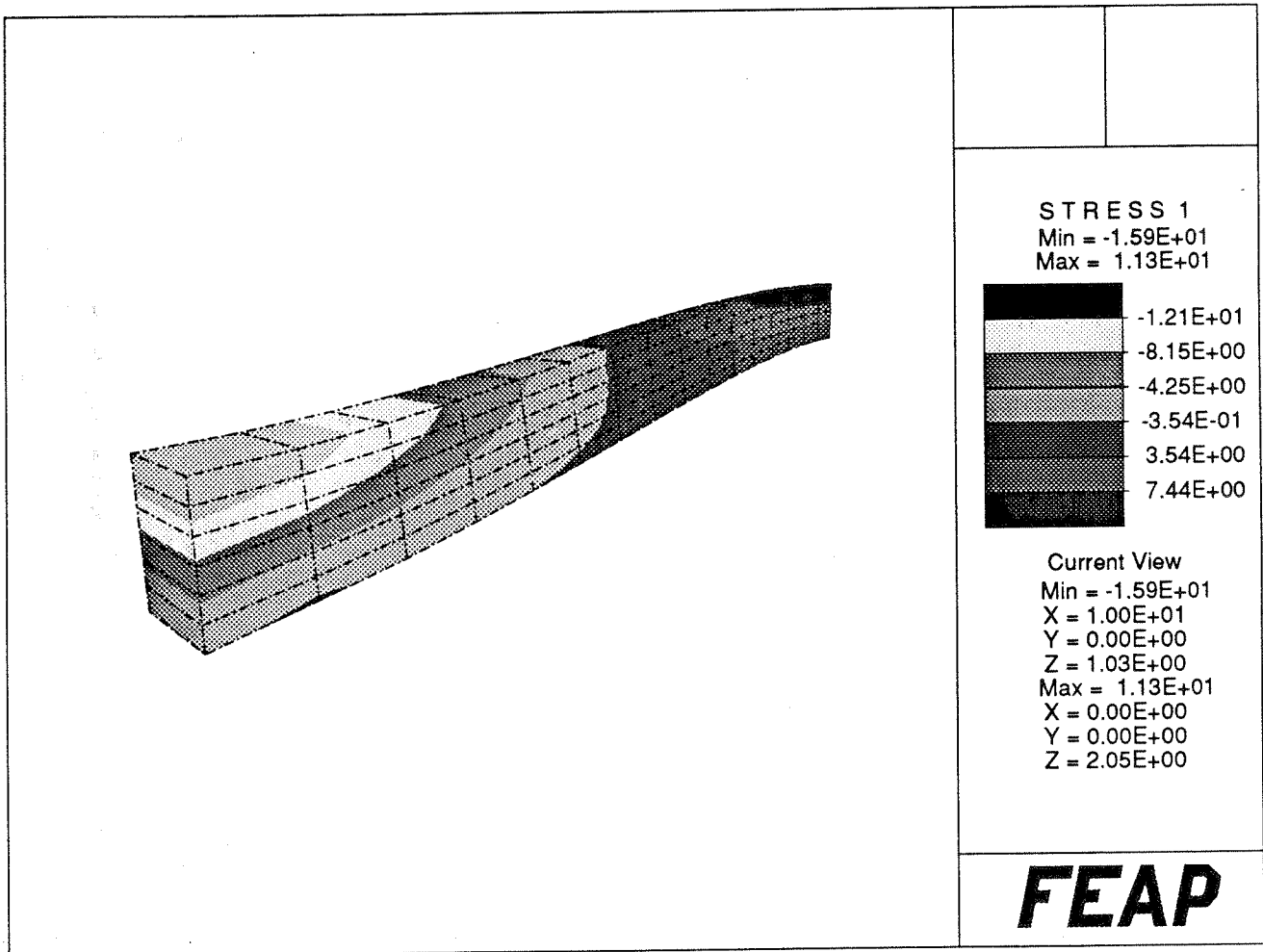
Figure 12: Clamped circular plate: three dimensional mesh in a deformed configuration.
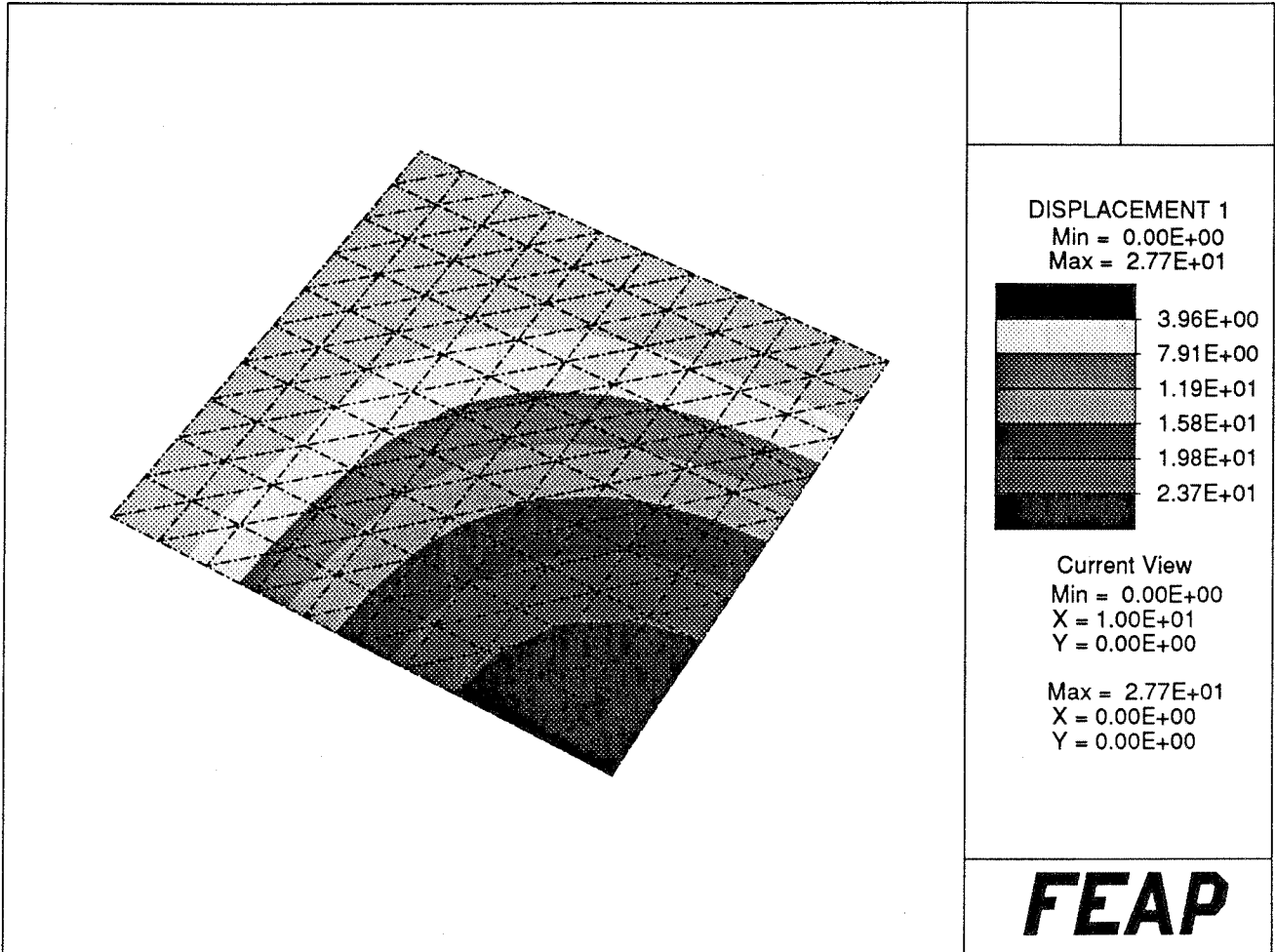The contour lines for the radial stress are also shown.
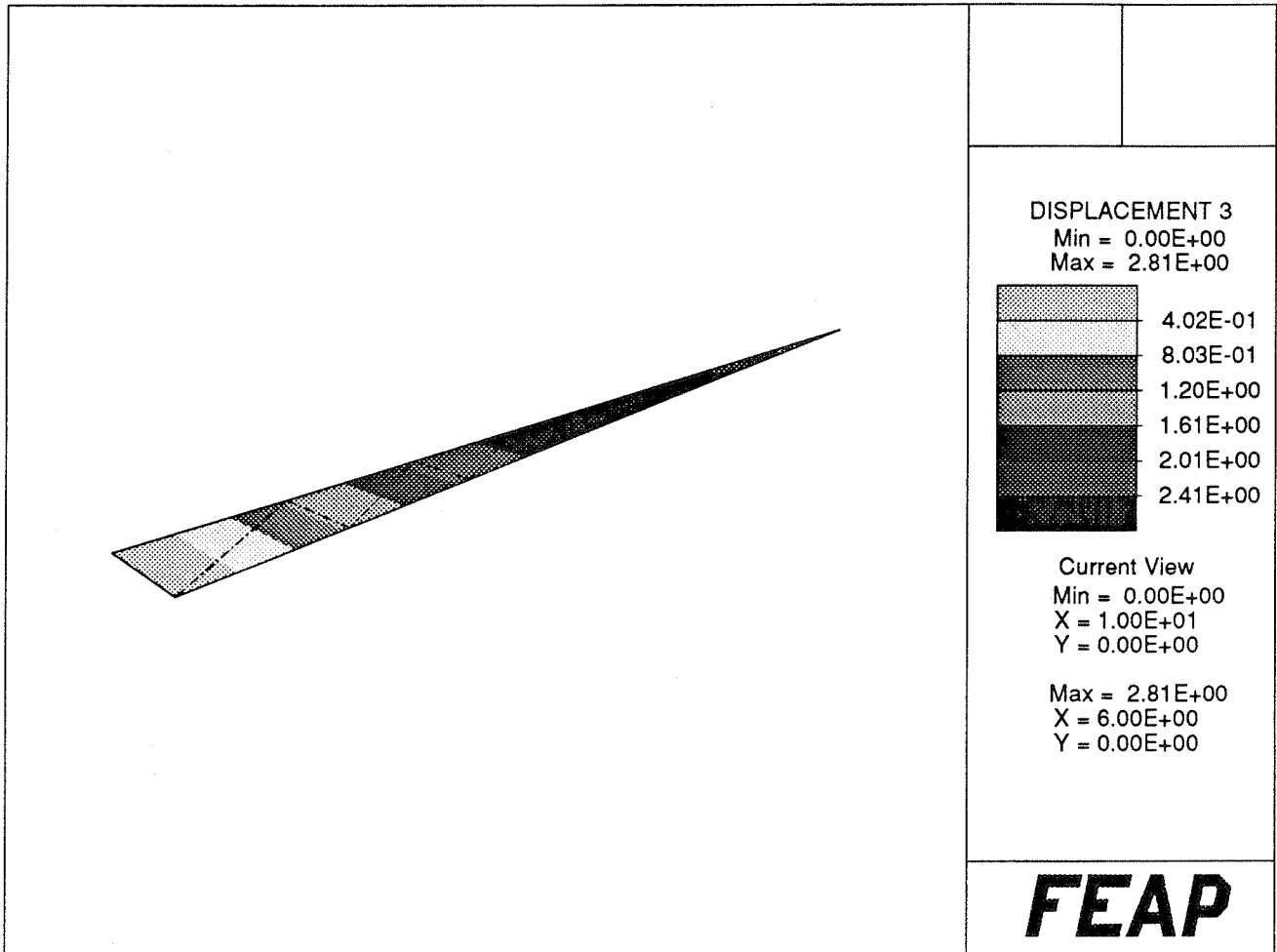
Figure 13: Clamped circular plate: two dimensional mesh in the undeformed configuration.
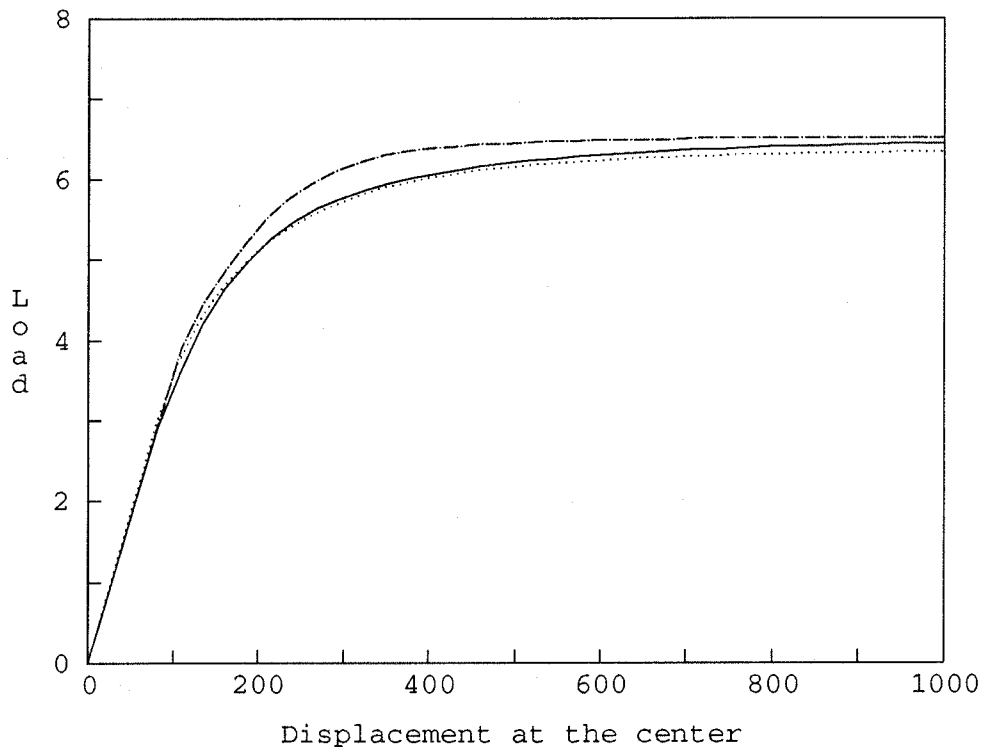The contour lines for the vertical displacement are also shown.
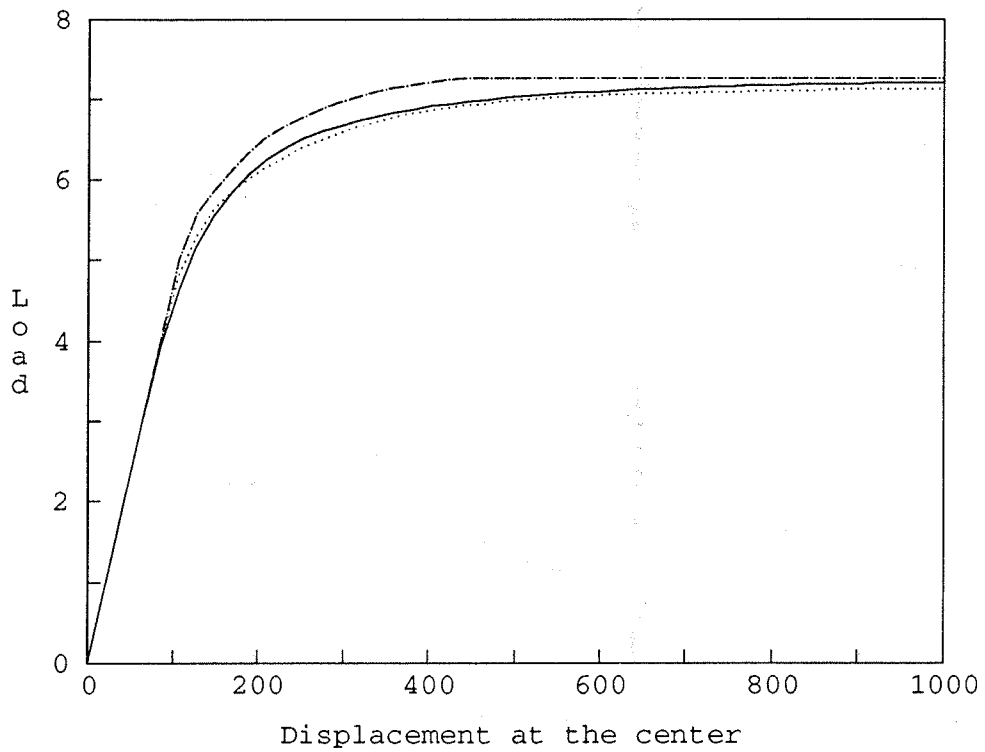
Figure 14: Clamped circular plate: limit load. Two dimensional analysis versus three dimensional analysis.
Transverse load versus displacement at the center for generalized plasticity plate model (continuous line), classical plasticity plate model (dot-dash line) and three-dimensional classical plasticity model (dotted line).
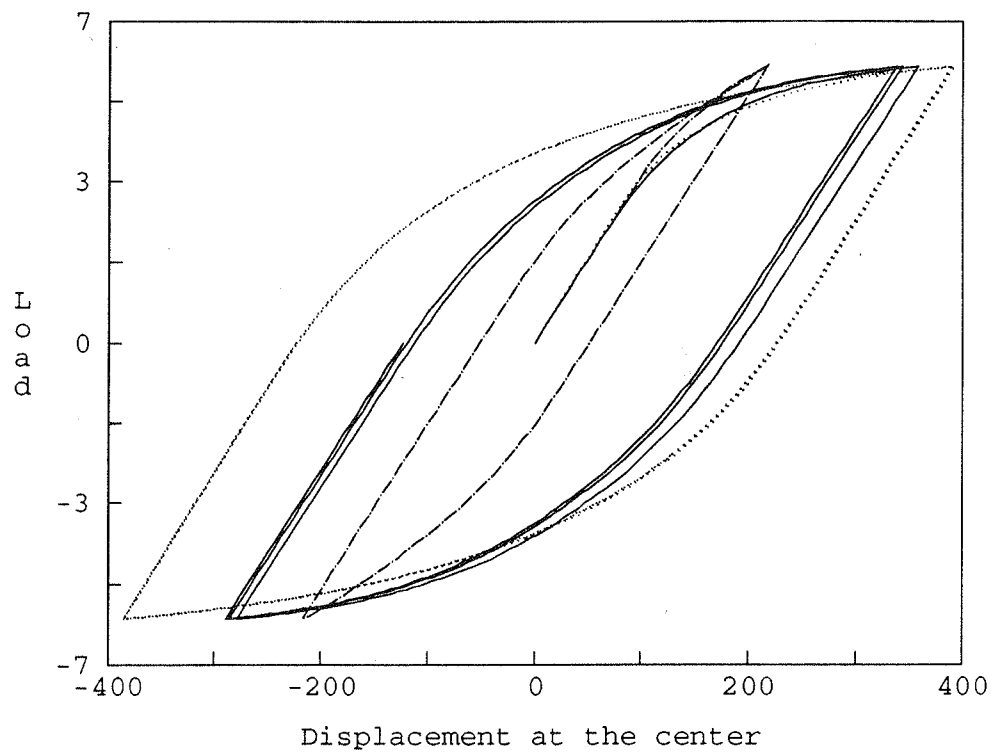
Figure 15: Clamped circular plate: cyclic load. Two dimensional analysis versus three dimensional analysis.
Transverse load versus displacement at the center for generalized plasticity plate model (continuous line), classical plasticity plate model (dot-dash line) and three-dimensional classical plasticity model (dotted line).

Figure 16: Clamped square plate: three dimensional mesh in a deformed configuration.

DISPLACEMENT 1
Min = 0.00E+00
Max = 2.77E+01

3.96E+00
7.91E+00
1.19E+01
1.58E+01
1.98E+01
2.37E+01

Current View
Min = 0.00E+00
X = 1.00E+01
Y = 0.00E+00

Max = 2.77E+01
X = 0.00E+00
Y = 0.00E+00

FEAP

Figure 17: Clamped square plate: two dimensional mesh in the undeformed configuration.

Figure 18: Clamped square plate: limit load. Two dimensional versus three dimensional analysis.
Transverse load versus displacement at the center for generalized plasticity plate model (continuous line), classical plasticity plate model (dot-dash line) and three-dimensional classical plasticity model (dotted line).

Figure 19: Clamped square plate: cyclic loading. Two dimensional versus three dimensional analysis.
Transverse load versus displacement at the center for generalized plasticity plate model (continuous line), classical plasticity plate model (dot-dash line) and three-dimensional classical plasticity model (dotted line).

List of Figures